Z-Pinch Chamber Assessment and Design

L. El-Guebaly, M. Sawan, I. Sviatoslavsky, P. Wilson,
G. Sviatoslavsky, G. Kulcinski

October 2005
(revised November 2006)

UWFDM-1283

FUSION TECHNOLOGY INSTITUTE

UNIVERSITY OF WISCONSIN

MADISON WISCONSIN

Z-Pinch Chamber Assessment and Design

L. El-Guebaly, M. Sawan, I. Sviatoslavsky,
P. Wilson, G. Sviatoslavsky, G. Kulcinski

Fusion Technology Institute
University of Wisconsin
1500 Engineering Drive
Madison, WI 53706

http://fti.neep.wisc.edu

October 2005
(revised November 2006)

UWFDM-1283

1. Introduction

The 2005 design is built on the previous 2004 study [1], focusing on more detailed analysis and advanced technology. An engineering scoping assessment has been developed for two candidate breeders: the Flibe (F_4Li_2Be) molten salt and the $Li_{17}Pb_{83}$ liquid metal. Identifying the design requirements, optimizing the components' dimensions, establishing the jet flow, determining the thermal and power cycle parameters, characterizing the radiation environment, and meeting the Z-pinch specific design needs were given considerable attention. The nuclear assessment has been a fundamental element of the Z-pinch design process. Certain features of the nuclear activity focused on areas unique to the Z-pinch, including breeding potential of jets and pool, chamber wall dimensions, damage profile at chamber wall, and life-cycle waste classification.

Section 2 documents the key design parameters and radiation limits that are essential for the nuclear assessments. Section 3 focuses on the nuclear assessment, explores the design space with a 1-D parametric study, and identifies self-consistent reference parameters using detailed 3-D analysis. A novel approach to establish the jet flow is presented in Section 4 along with the thermal and power cycle parameters. Section 5 documents the rationale for selecting the chamber wall material based on the low-level waste requirement. An interesting comparison between the candidate breeders is given in the last section, highlighting the fundamental differences in performance and the benefits and drawbacks of each breeder.

2. Design requirements and radiation limits

We began the chamber assessment by identifying a set of nuclear objectives. These are summarized below:

Design Requirements	Impact and limits*
Closed tritium fuel cycle	Calculated TBR $\geq$ 1.1
Structural integrity	200 dpa to steel-based structure at end-of-life
Thermal conversion efficiency	> 40% to enhance net electric power
Minimal heat leakage	< 1% nuclear heat leakage from chamber wall
Reweldability limit	1 helium appm for steel-based structure
Only low-level waste	Class A or C LLW with careful material choice
Plant lifetime	40 FPY
Plant availability	85%

* Acronyms: TBR for tritium breeding ratio, dpa for displacement per atom, appm for atom part per million, LLW for low-level waste, FPY for full power year.

A tritium-breeding ratio (TBR) of 1.1 assures tritium self-sufficiency for the Z-pinch machine. The 10% breeding margin accounts for the uncertainties in the cross section data, approximations in geometric model, losses due to T reprocessing and decay, and T supply for future power plants. The net TBR at the beginning of plant operation may range between 1.01 and 1.2 and a flexible blanket design could adjust the net TBR to 1.01. In case of over-

breeding (net TBR > 1.01), the TBR can be reduced by depleting the Li of the breeder. In case of under-breeding (net TBR < 1.01), the TBR can be increased by Li enrichment and/or adding more jets.

The ability to identify the life-limiting criteria for the steel structural is a key factor to determine accurately the service lifetime of the chamber wall. Historically, the atomic displacement, thermal and mechanical stresses, and/or thermal creep have led to a failure mechanism, prematurely ending the service lifetime of structural components. The dpa limit ranges between 100 and 200 dpa, depending on the steel type. In the absence of firm experimental data for advanced steels, optimistic criteria normally determine the limits and account for future improvements to existing materials. For the Z-pinch design, we adopted the high 200 dpa limit in concert with similar ground rules being considered for advanced fusion designs, such as ARIES.

A key engineering aspect of the Z-pinch machine is the potential for high thermal conversion efficiency (40-50%) with advanced steel-based structure that is capable of operating at high temperature (550-800^{o}C). The nuclear heat leakage from the chamber wall to the surroundings must remain below 1% (~ 3 MW_{th}) to enhance the thermal power. If there is a need to cut and reweld the chamber wall during plant operation, the helium production level should not exceed 1 appm at the chamber wall. No high-level waste should be produced to avoid the deep geological burial.

3. Chamber nuclear assessment

Addressing the nuclear issues, it is prudent to routinely check if the design requirements are met when the design choices are made. We started the analysis with 1-D scoping analyses to examine the breeding capacity of the Flibe and LiPb candidate breeders and roughly estimate the jet parameters (thickness and Li enrichment) that protect the chamber wall for the plant life (40 FPY). Next, the chamber wall size was determined to essentially limit the nuclear heat leakage to less than 1%. Because of the strict low-level waste (LLW) requirement, we included the activation assessment at an early stage during the design process and an important decision was made regarding the selection of the chamber wall material. Finally, we specified the reference nuclear parameters with a detailed 3-D computational model of the chamber jets, pool, and wall. The deliverables were the jet size, Li enrichment, overall TBR, total thermal power, nuclear heat load to all components, radiation damage profile at wall segments and their service lifetimes. The entire nuclear assessment proceeded interactively with guidance from the thermal analysis.

The 3 GJ design calls for 10 chambers operating at a rep rate of 0.1 Hz. Figure 1 displays the spectral neutron flux outside the target. The softer neutrons result from the interaction of the 14 MeV source neutrons with the target materials (Be, CH, and Au). Considerable softening occurs as neutrons travel through and interact with the breeder jets, as Fig. 2 illustrates.

For the nuclear assessment, it is essential to understand the evolution of the liquid breeder with time following the target implosion. The sequence of events indicates the geometry of the jets/pool hardly changes before the arrival of neutrons. The x-rays drive strong shock

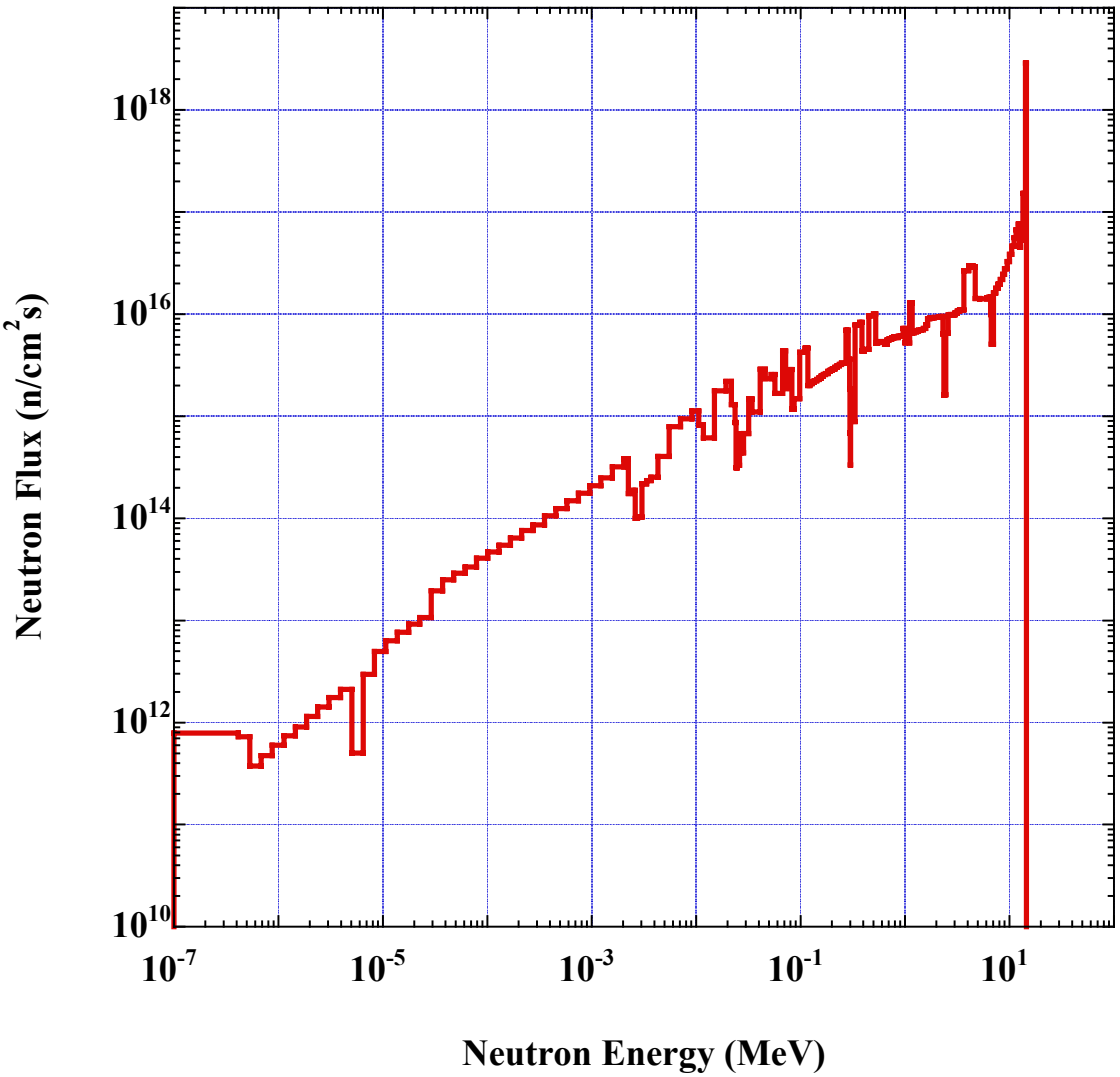

Fig. 1. Neutron spectrum outside the Z target for 175 neutron group structure.

waves into the liquid breeder. They behave differently, depending on the chamber condition (with or without gas). The neutrons deposit their energy volumetrically in the breeder and underlying structure. The neutron heating causes pressurization and rapid expansion of the jets/pool. The hydromotion leads to splashing of the liquid breeder and breakup of the entire jets and pool. Per R. Peterson (SNL), the sequence of events can be described as follows:

- Gas in chamber:
  - If gas is thick enough to stop x-rays, fireball will be formed that releases energy slowly enough that liquid vaporization might be avoided
  - Strong shock in gas will occur
- No Gas in Chamber:
  - X-rays rapidly deposit their energy at liquid surface:
    - Vaporizing few microns
    - Producing vapor that rapidly blows off of liquid surface

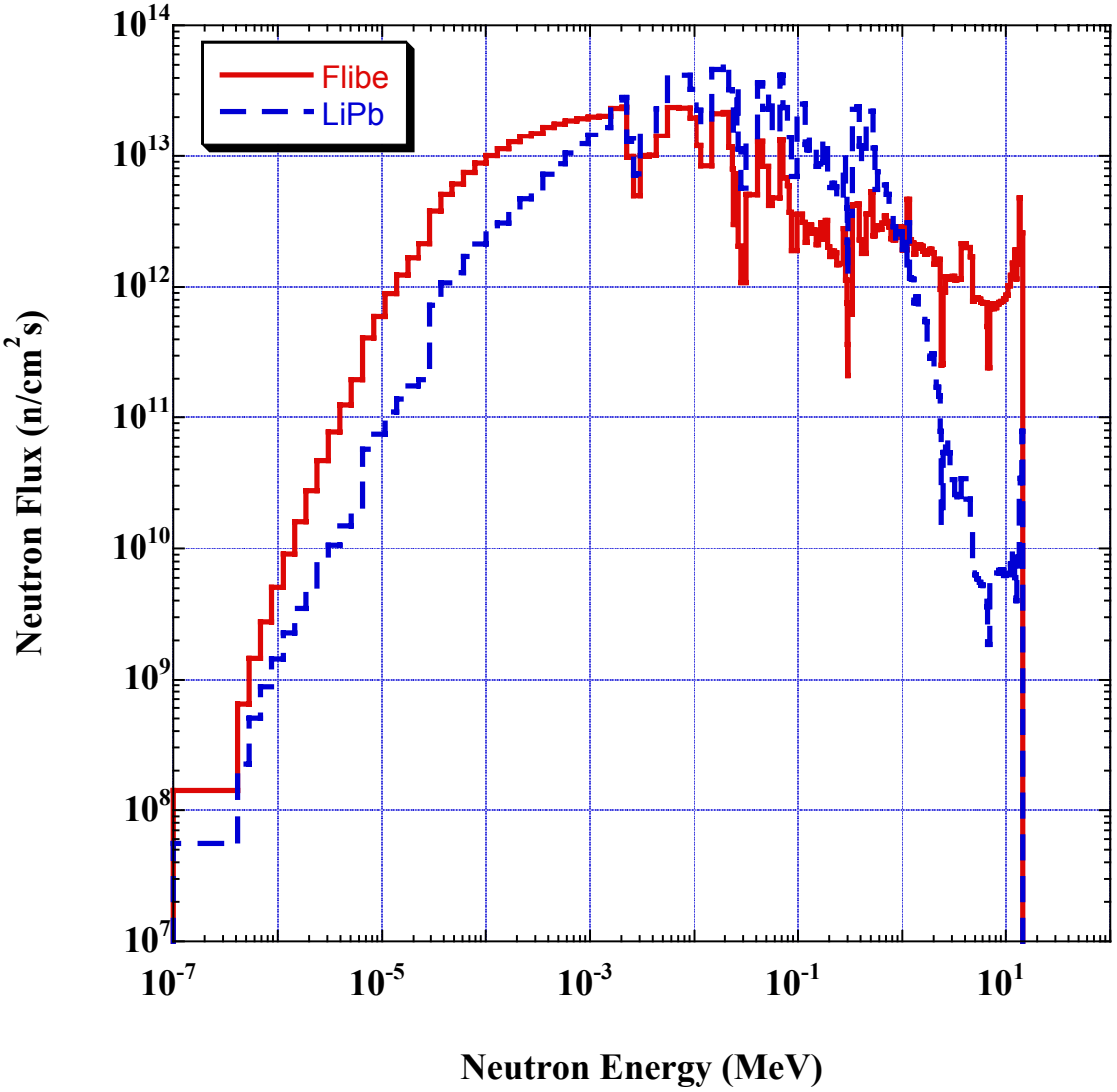

Fig. 2. Neutron spectrum (for 175 neutron group structure) at inner surface of chamber wall for Flibe and LiPb breeders.

- Driving strong shock waves into liquid

- Geometry of liquid hardly changes before neutron arrival
- Neutrons deposit their energy volumetrically, causing rapid expansion of liquid
- Vapor:
  - Cools down during expansion
  - Stops ions
  - Gets reheated by ions
  - Radiates heat, vaporizing more liquid $\Rightarrow$ ions heat liquid indirectly
- Hydro-motion leads to splash and break-up of liquid.

The candidate steels for the chamber wall are A-286 [2] and F82H [3,4]. The chemical composition and elemental impurities are given in Table 1. Note that the impurities for the A-286 steel are missing and its high Mo content may cause activation problems. There is a class of low activation, radiation-resistant ferritic steel (FS) alloys that offer low neutron-induced swelling, low thermal expansion coefficient, high resistance to irradiation creep, and high range of operating temperatures. An example of advanced FS suitable for fusion applications includes the nanocomposited oxide dispersion strengthening (ODS) FS [5].

Table 1. Chemical composition and impurities of A-286 and F82H steels.

	A-286 Steel	**F82H Steel**
B	0.006	
C	0.04	0.1
Al	0.15	14e-4
P	0.015	
S	0.002	
Si	0.2	
Ti	2.1	
V	0.3	0.2
Cr	14.5	7.5
Mn	0.2	
Fe	56.237	90.116
Co		28e-4
Ni	25	474e-4
Cu		100e-4
Nb		3.3e-4
Mo	1.25	21e-4
Pd		0.05e-4
Ag		0.1e-4
Cd		0.4e-4
Ta		0.02
W		2.0
Os		0.05e-4
Ir		0.05e-4
Bi		0.2e-4
Eu		0.05e-4
Tb		0.02e-4
Dy		0.05e-4
Ho		0.05e-4
Er		0.05e-4
U		0.05e-4

3.1 1-D parametric study

Preceding the 3-D analysis, a series of parametric 1-D analysis using the DANTSYS code [6] was established to guide the design process and identify the initial configuration for the 3-D analysis. The FENDL-2 data library [7] was employed for the 1-D analysis, 175 neutron and 42 gamma group structure with P_3-S_8 approximation. The 1-D spherical model included the essential elements that impact the nuclear parameters: the details of the target at burn, thin layer of the RTL, breeder jets (100% dense) at 1 m from target center, and chamber wall. The variable-size gap behind the jets was eliminated to help estimate the peak radiation damage at the chamber wall.

The sensitivity of TBR, dpa, He production, and heat leakage with the thickness of the candidate breeders (F_4Li_2Be and $Li_{17}Pb_{83}$ with natural Li enrichment) was examined. Figures 3-7 display the results for the F_4Li_2Be breeder with natural Li enrichment. The following observations can be made:

Figs. 3 and 4:

- 42 cm Flibe (F_4Li_2Be, 100% dense with natural enrichment) protects the wall for plant life (dpa = 200) and over-breeds tritium (TBR > 1.1).
- A-286 steel results in slightly higher breeding and damage.
- Variations:
  - Larger target-to-Flibe distance $\Rightarrow$ slightly more breeding
  - Less dense Flibe (with adjusted thickness) $\Rightarrow$ slightly lower breeding
  - Larger Flibe-to-wall gap $\Rightarrow$ slightly lower breeding

Fig. 5:

- No significant change to breeding and wall damage with Flibe enrichment.
- 3-D analysis should determine reference Flibe thickness and enrichment.

Fig. 6:

- A-286 steel generates more helium (factor of 3) due to boron alloying element. Boron may affect other properties, such as swelling, creep, etc.
- Chamber wall cannot be rewelded at any time during operation (>> 1 He appm).
- Mechanical attachments or other means should be considered for wall assembly behind jets in particular.

Fig. 7:

- 42 cm Flibe and 30 cm wall recover 99% of total nuclear heating.

Figures 8-12 display the results for the $Li_{17}Pb_{83}$ breeder with natural Li enrichment. Several observations are notable:

Figs. 8 and 9:

- 80 cm $Li_{17}Pb_{83}$ (100% dense with natural enrichment) meets the breeding requirement (TBR = 1.1) and protects the wall for plant life (dpa = 200).
- A-286 steel results in slightly higher breeding and damage.

Fig. 10:

- Enrichment increases breeding significantly and reduces wall damage.
- 3-D analysis should determine reference LiPb thickness and enrichment.

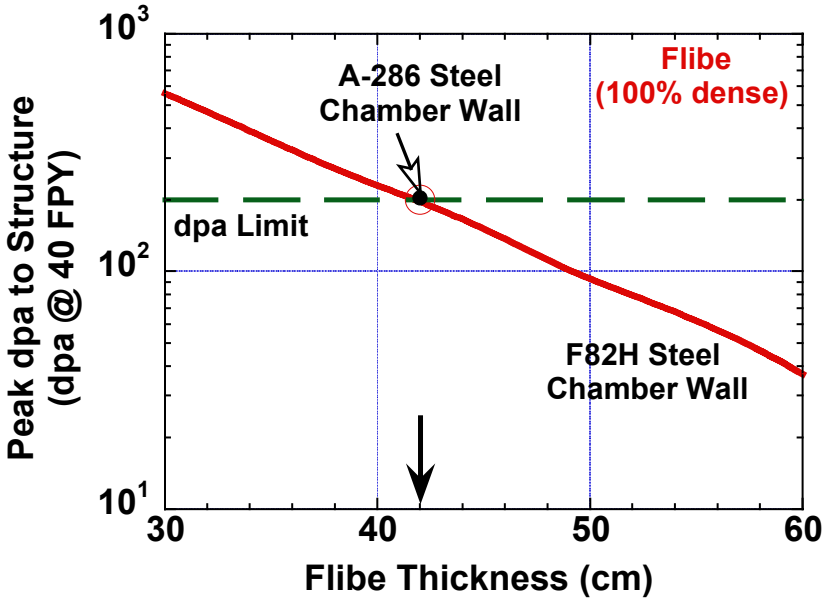

Fig. 3. Variation of dpa at chamber wall with Flibe thickness.

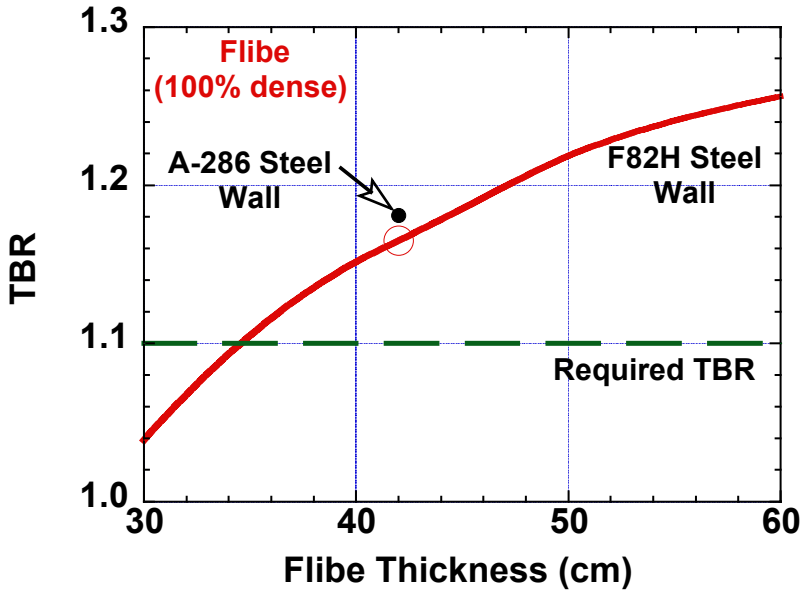

Fig. 4. The increase in TBR with Flibe thickness.

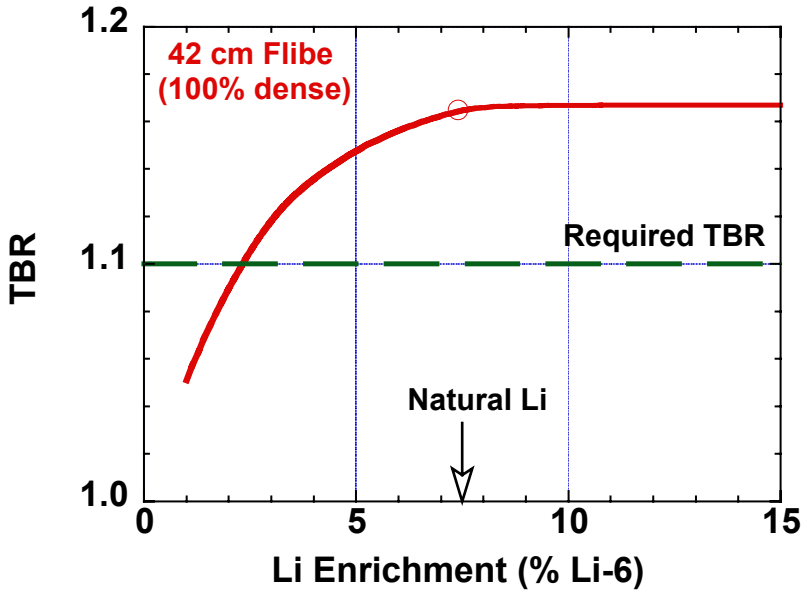

Fig. 5. TBR versus Li enrichment of Flibe.

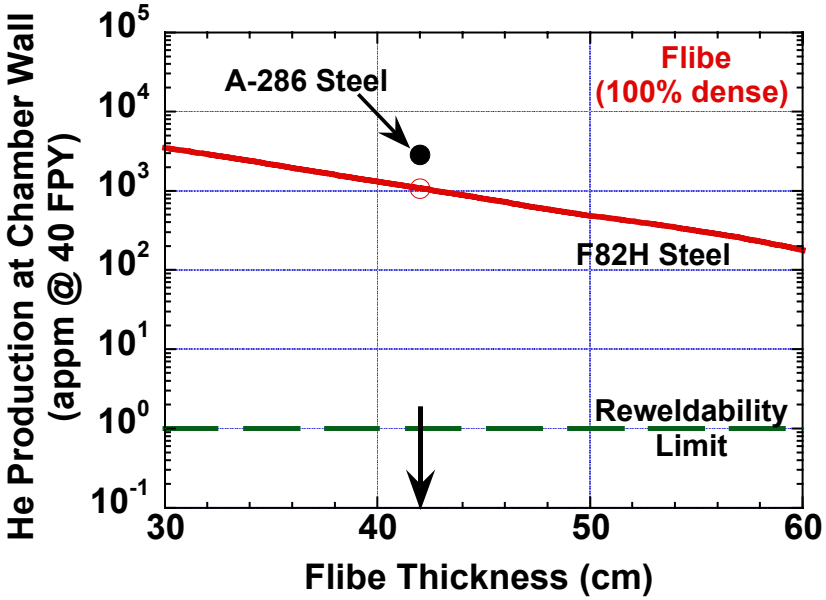

Fig. 6. Sensitivity of He production at chamber wall to Flibe thickness.

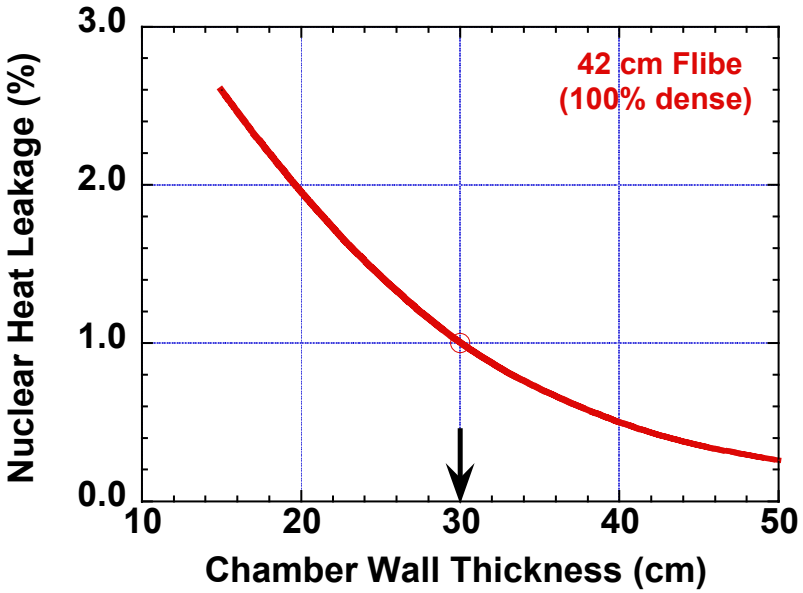

Fig. 7. The reduction of heat leakage with chamber wall thickness.

Fig. 11:

- A-286 steel generates more helium (factor of 220) due to boron alloying element.
- Chamber wall cannot be rewelded at any time during operation (>> 1 He appm).
- Mechanical attachments or other means should be considered for wall assembly behind jets in particular.

Fig. 12:

- 80 cm LiPb and 50 cm wall recover 99% of total nuclear heating.

This concludes the 1-D scoping assessment. In the following section, the 3-D analysis will call for measures to enhance the engineering aspect of the design based on the overall nuclear performance. Optimization of the jet dimensions and breeder parameters, definition of the heat load to individual components, and characterization of the radiation damage profile were given considerable attention during the 3-D study.

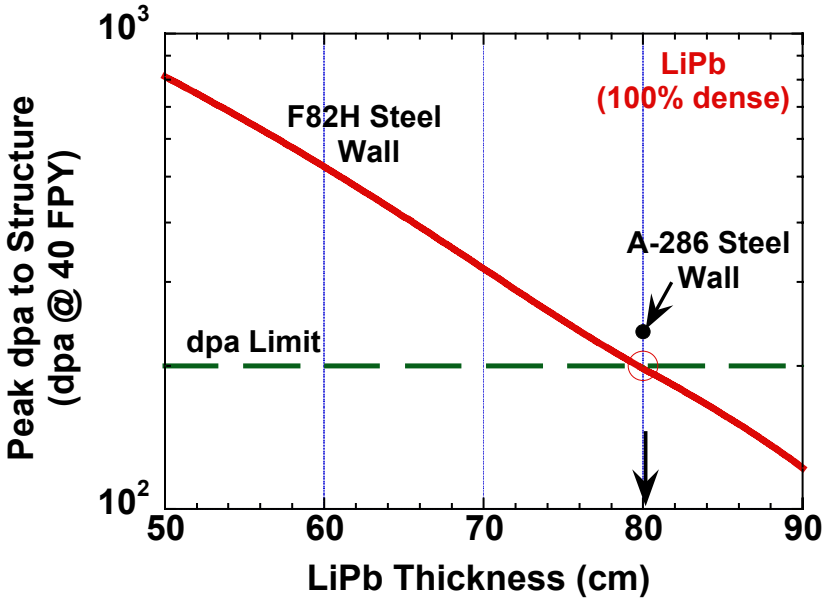

Fig. 8. Variation of dpa at chamber wall with LiPb thickness.

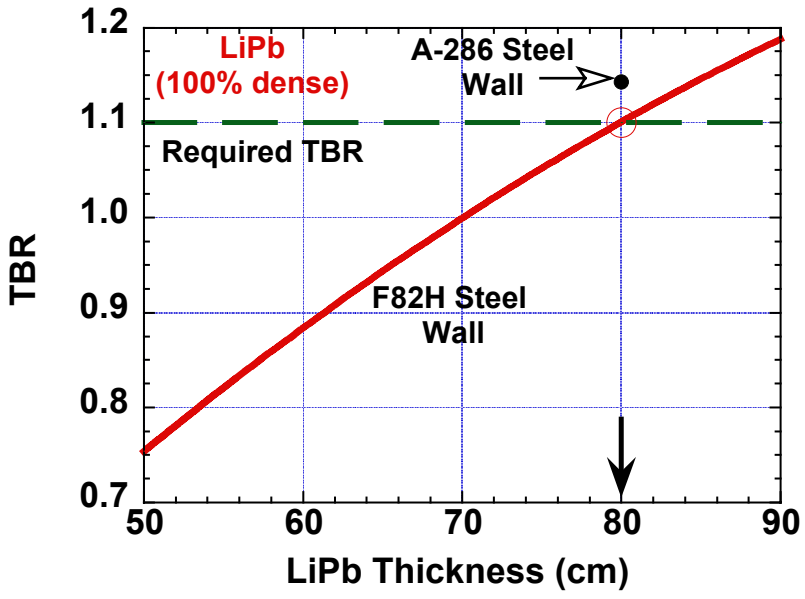

Fig. 9. The increase in TBR with LiPb thickness.

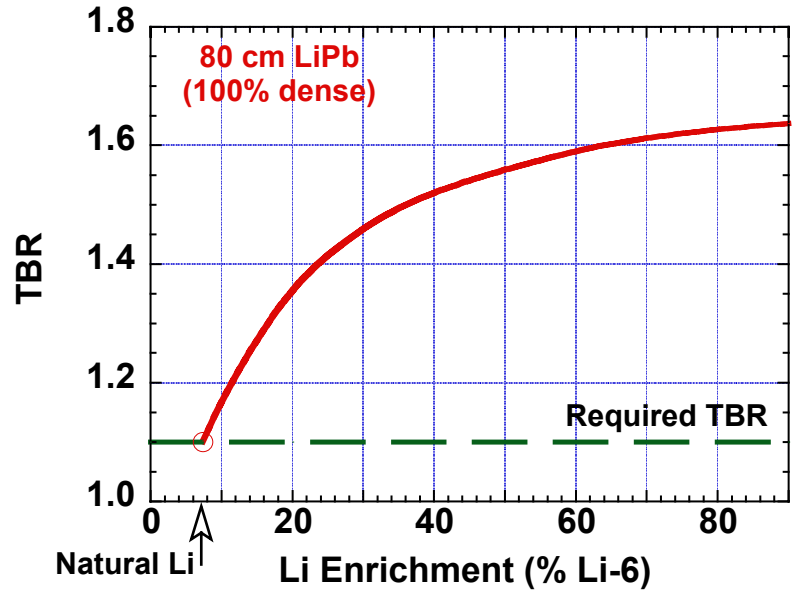

Fig. 10. TBR versus Li enrichment of LiPb.

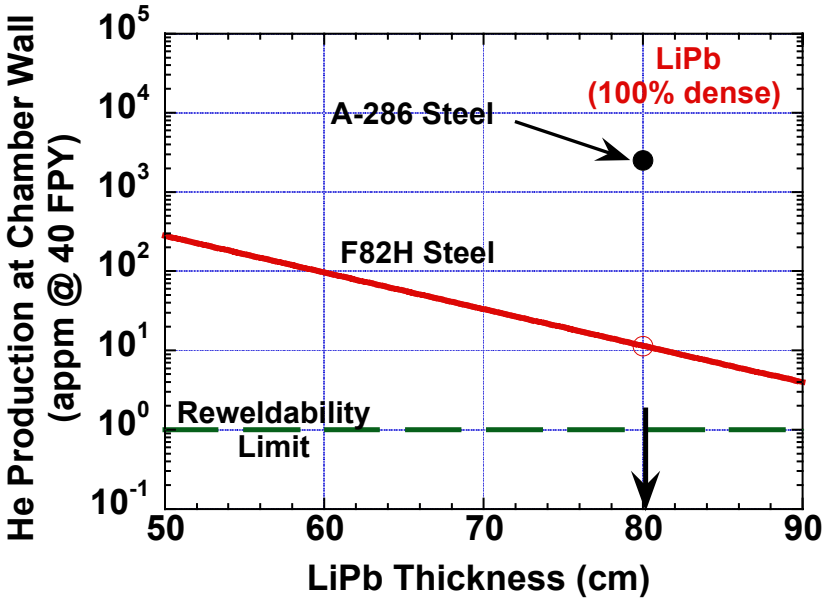

Fig. 11. Sensitivity of He production at chamber wall to LiPb thickness.

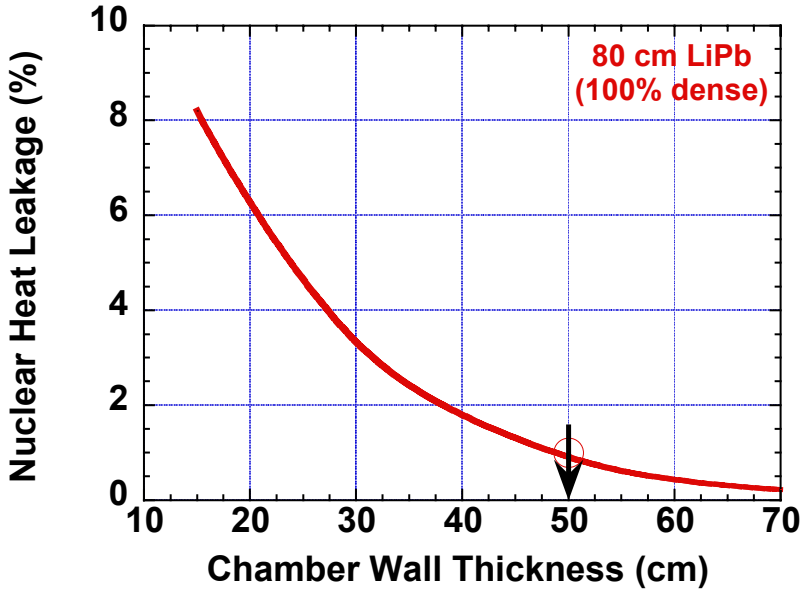

Fig. 12. The reduction of heat leakage with chamber wall thickness.

3.2 3-D nuclear analysis

3.2.1 Calculation procedure

Detailed three-dimensional (3-D) neutronics calculations have been performed for the chamber using the latest version of the continuous energy, coupled neutron-gamma Monte Carlo code MCNP, version 5 [8] along with nuclear data based on the most recently released evaluation FENDL-2.1 [9]. The elliptical chamber concept shown in Fig. 13 was modeled. The chamber has an inner diameter of 10 m and a height of 6 m. The double-layered RTL is made of carbon steel. The layers were modeled as two truncated cones with the outer layer being 0.9 mm thick and the inner layer having a thickness of 0.5 mm. A 10 mm gap exists between the two RTL layers. The imploded target radial build and composition with a ρR of 3 was included in the model at the lower tip of the RTL. The target is located at 0.5 m above the chamber geometrical center. The target configuration at ignition was modeled by a set of spherical shells. The compressed DT core has a radius of 0.57 mm and is surrounded by 8.3 mm thick Be, 0.11 mm thick CH, and 1.65 mm thick Au shells. 14.1 MeV source neutrons were sampled uniformly from the DT spherical core.

The liquid jets and pool breed the tritium required to fuel the targets, absorb the energy carried by neutrons, x-rays, and ion debris emitted from the target, and shield the structural chamber wall from neutron damage. We performed the 3-D calculations for the two liquid breeder options considered. Fig. 14 gives the 3-D geometrical model used for the chamber

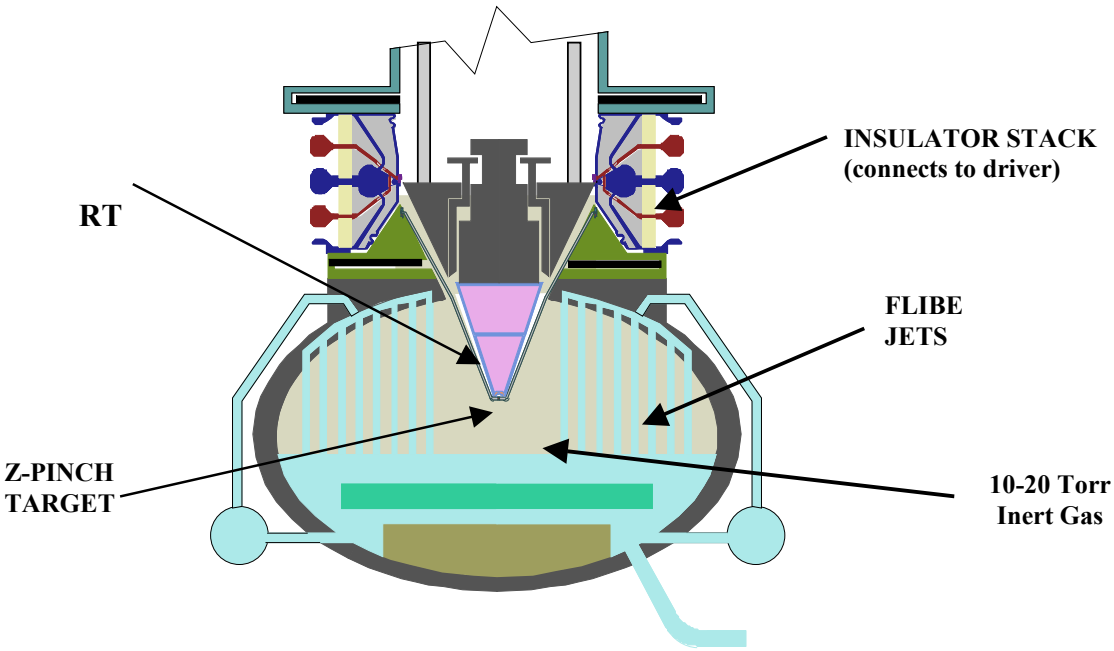

Fig. 13. Elliptical Z-pinch IFE chamber concept.

that utilizes the molten salt Flibe as the breeding liquid. The jet zone has an inner radius of 1 m. Eight rows of Flibe jets are utilized with the outer surface of the last row at a radius of 2.1 m. The packing fraction of the jets is 37%. The pool depth surface is at 1 m below the chamber center implying that the maximum pool depth is 2 m. Gas is bubbled in the pool for shock mitigation. A density factor of 0.8 is used for the Flibe in the pool. Flibe foam at 0.1 density factor is used to fill the RTL cone. Natural lithium is used in the Flibe. The chamber wall is 0.3 m thick and is made of the low activation ferritic steel alloy F82H [3,4]. The nozzle zone of the chamber wall above the Flibe jets consists of 66% F82H and 34% Flibe. The insulator stack above the chamber is simulated in the 3-D model by a zone made of epoxy to evaluate the expected insulator radiation environment.

Figure 13 shows the 3-D geometrical model used for the chamber that utilizes the lithium lead eutectic ($Li_{17}Pb_{83}$) as the breeding liquid. A thicker jet zone is needed with LiPb to provide adequate shielding for the chamber wall. Twelve rows of jets are used with the surface of the outer row at a radius of 2.7 m. The lithium is slightly enriched to 20% Li-6. The chamber wall thickness is increased to 0.5 m to reduce the energy leakage from the chamber. LiPb foam with 0.1 density factor is used inside the RTL cone. Several splitting surfaces have been added to allow for utilizing the geometry splitting with Russian Rolette variance reduction techniques [9] needed to reduce the statistical uncertainties in the calculated nuclear parameters. The calculations have been performed with 100,000 source particles yielding statistical uncertainties less than 0.5% for integral quantities and 2% for local parameters. The results were normalized to a fusion power of 300 MW per chamber (DT target yield of 3 GJ and repetition rate of 0.1 Hz).

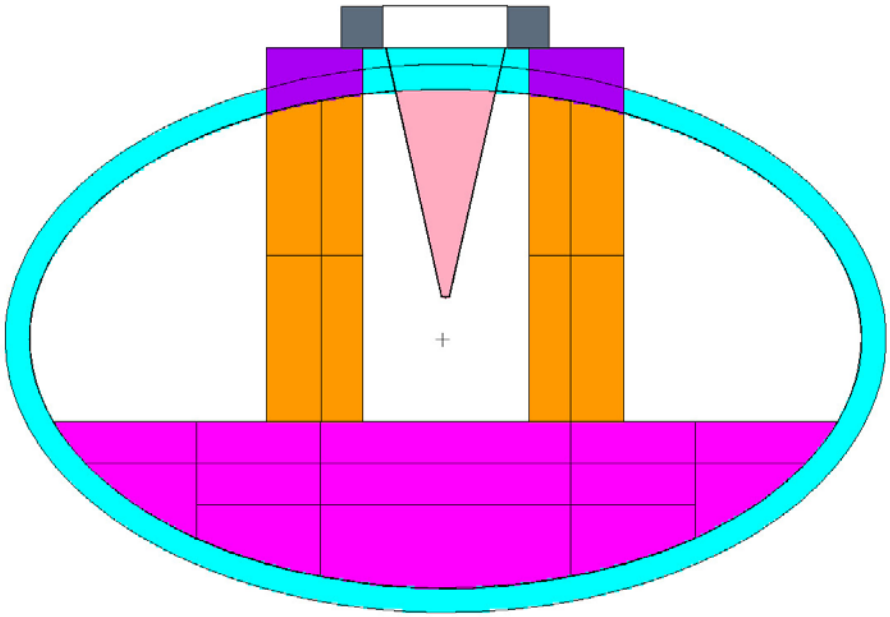

Fig. 14. The MCNP 3-D model for the chamber with Flibe liquid breeder.

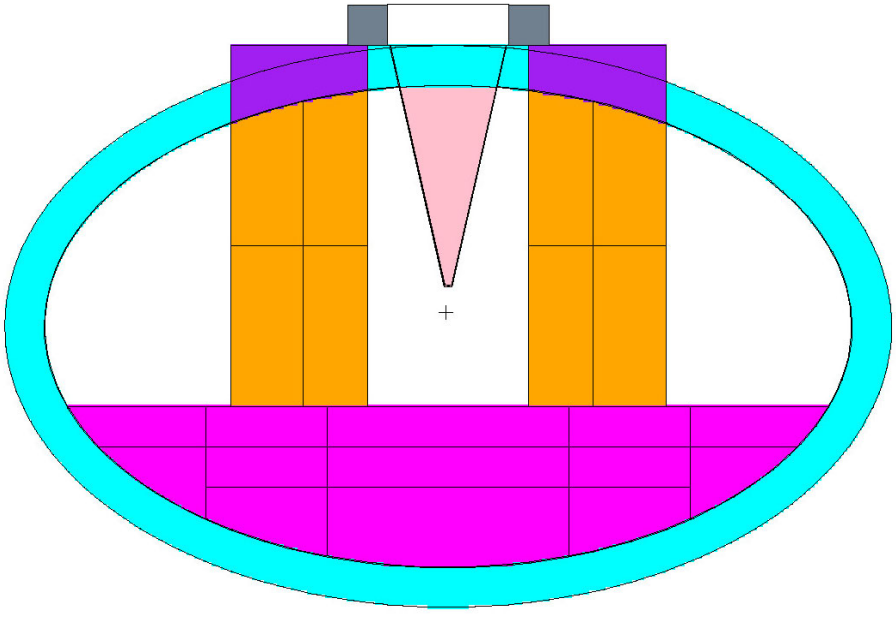

Fig. 15. The MCNP 3-D model for the chamber with LiPb liquid breeder.

3.2.2 Tritium breeding

Tritium production in the different breeder zones of the chamber was determined for the two breeder options. The results are given in Table 2. It is clear that most of tritium breeding occurs in the jet zone although the amount of breeder in the jets is much smaller than that in the pool. The reason is that the jets are exposed to 88% of the source neutrons emanating from the target while the pool is exposed directly to only 9% of the source neutrons. The overall tritium breeding ratio (TBR) is >1.1 in both cases implying that both breeder options have the potential for achieving tritium self-sufficiency.

Table 2. Tritium production in the different breeder zones of the chamber

	Tritium Production per Fusion	
	Flibe Breeder	LiPb Breeder
Jets	0.840	0.711
Nozzle Zone	0.019	0.053
Pool	0.246	0.362
RTL Foam	0.011	0.005
Overall TBR	**1.116**	**1.131**

3.2.3 Nuclear Heating

Nuclear energy deposited by neutrons and gamma photons in the chamber components was determined for the two designs with Flibe and LiPb. Table 3 lists the amount of nuclear heating in the target layers for the 3 GJ DT yield shot. These results were found to be independent of the breeder choice. Adding the amount of nuclear heating in the target to the 3.5 MeV carried by the alpha particle from the fusion reaction implies that the total energy carried by x-rays and ion debris per DT fusion is 4.987 MeV. These results indicate that out of the 3 GJ DT target yield 2.147 GJ is carried by neutrons and 0.853 GJ is carried by x-rays and ion debris.

Table 3. Nuclear heating in target layers

	MeV/fusion	MJ per 3 GJ DT yield shot
DT core	1.476	251.59
Be shell	9.62×10^{-3}	1.64
CH shell	2.95×10^{-4}	0.05
Au shell	4.13×10^{-4}	0.07
TOTAL	**1.487**	**253.35**

Table 4 gives the breakdown of the amount of nuclear heating deposited in the chamber components for each 3 GJ yield shot with the Flibe breeder. The values of surface heating deposited by x-rays and ion debris at component surfaces facing the target are also given as well as the total thermal energy in each of the chamber components. The overall energy

multiplication defined as the ratio of the total thermal power to the fusion power is 1.115. The results for the chamber with LiPb breeder are given in Table 5. The overall energy multiplication in this case is 1.187 which is ~6.5% higher than that with Flibe.

Table 4. Nuclear heating and total thermal energy in Flibe chamber components

	Nuclear Heating (GJ/shot)	X&D Heating (GJ/shot)	Thermal Energy (GJ/shot)
Jets	1.798	0.748	2.546
Pool	0.402	0.072	0.474
Chamber Wall	0.139	0.000	0.139
Nozzle Zone	0.062	0.000	0.062
RTL Support Structure	0.054	0.020	0.074
RTL	0.008	0.010	0.018
RTL Foam	0.033	0.000	0.033
Total	**2.496**	**0.850**	**3.346**

Table 5. Nuclear heating and total thermal energy in LiPb chamber components

	Nuclear Heating (GJ/shot)	X&D Heating (GJ/shot)	Thermal Energy (GJ/shot)
Jets	1.624	0.748	2.372
Pool	0.494	0.072	0.566
Chamber Wall	0.320	0.000	0.320
Nozzle Zone	0.158	0.000	0.158
RTL Support Structure	0.084	0.020	0.104
RTL	0.007	0.010	0.017
RTL Foam	0.023	0.000	0.023
Total	**2.710**	**0.850**	**3.560**

The pulsed nature of inertial fusion leads to sudden energy deposition in the liquid resulting in instant pressurization and disassembly with possible high speed acceleration of fluid masses inside the chamber. This phenomenon is referred to as isochoric heating. To help assess the problem we determined the distribution of energy deposition per unit volume of the fluid surrounding the target during each pulse. The results are shown in Figs. 16 and 17 for Flibe and LiPb, respectively. LiPb has higher nuclear heating per unit volume at the front zones but lower values at the back zones compared to Flibe. The mesh tally capability of MCNP5 was used to calculate the detailed distribution (5 cm x 5 cm mesh) of the isochoric heating in the Flibe jets (Fig. 18).

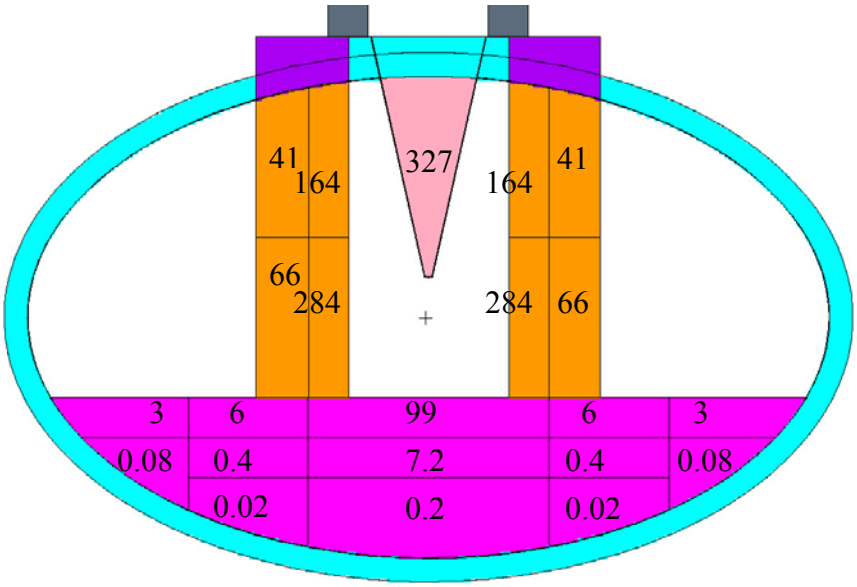

Fig. 16. Volumetric heating per shot (J/cm^3) in Flibe.

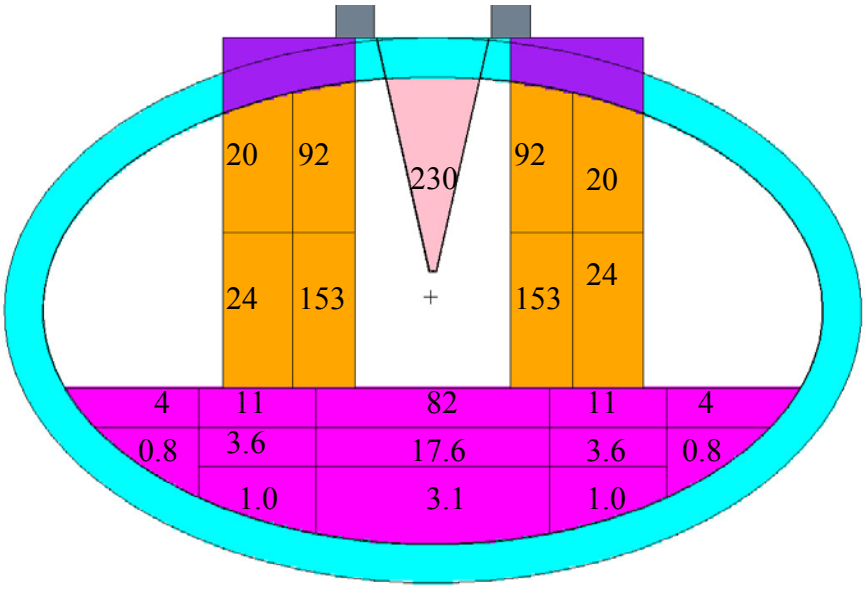

Fig. 17. Volumetric heating per shot (J/cm^3) in LiPb.

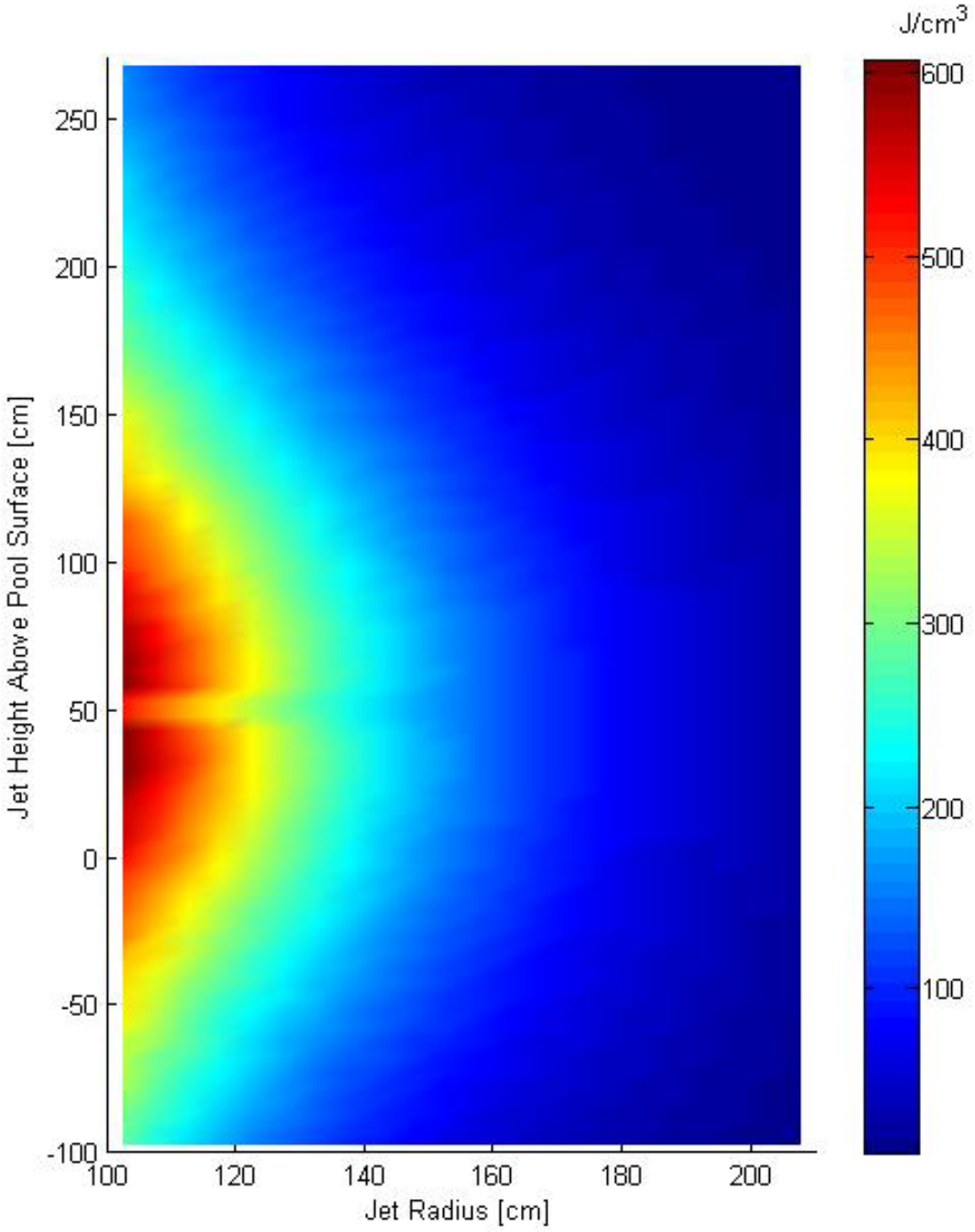

Fig 18. Detailed spatial distribution of volumetric heating in Flibe jet.

3.2.4 Radiation damage to chamber wall

3-D neutronics calculations were performed to determine the variation of damage rate at the inner surface of the chamber wall for both designs with Flibe and LiPb breeders. Fig. 19 gives the cumulative dpa rate along the inner surface of the chamber starting from the bottom of the pool and ending at the top of the chamber behind the RTL. A plant lifetime of 40 full power years (FPY) was assumed. The results for chambers with Flibe and LiPb are included for comparison. Radiation damage in the chamber wall is about a factor of 2 higher with LiPb. The largest chamber damage occurs at the unshielded area between the RTL and the jets. Based on a lifetime radiation damage limit of 200 dpa, the chamber wall is expected to be a lifetime component except for the top part starting in the nozzle zone. The nozzle zone of the chamber wall should be replaced once in the case of Flibe or three times in the LiPb design. The RTL support structure needs to be replaced at a factor of ~2 more frequent rates. Fig. 20 illustrates the lifetime for the different chamber regions for both the Flibe and LiPb designs. To assess the reweldability of the chamber wall, we determined the cumulative helium production at the inner surface of the chamber wall. The results are shown in Fig. 21 for the two breeder options. Helium production in the chamber wall is lower with LiPb. Based on a rewelding limit of 1 He appm, the part of the chamber wall below the LiPb pool is reweldable. On the other hand, with Flibe, only the part of the chamber wall that is ~20 cm below the pool surface can be rewelded. Hence, although most of the chamber wall is a lifetime component, rewelding is allowed only in a small part below the breeder pool.

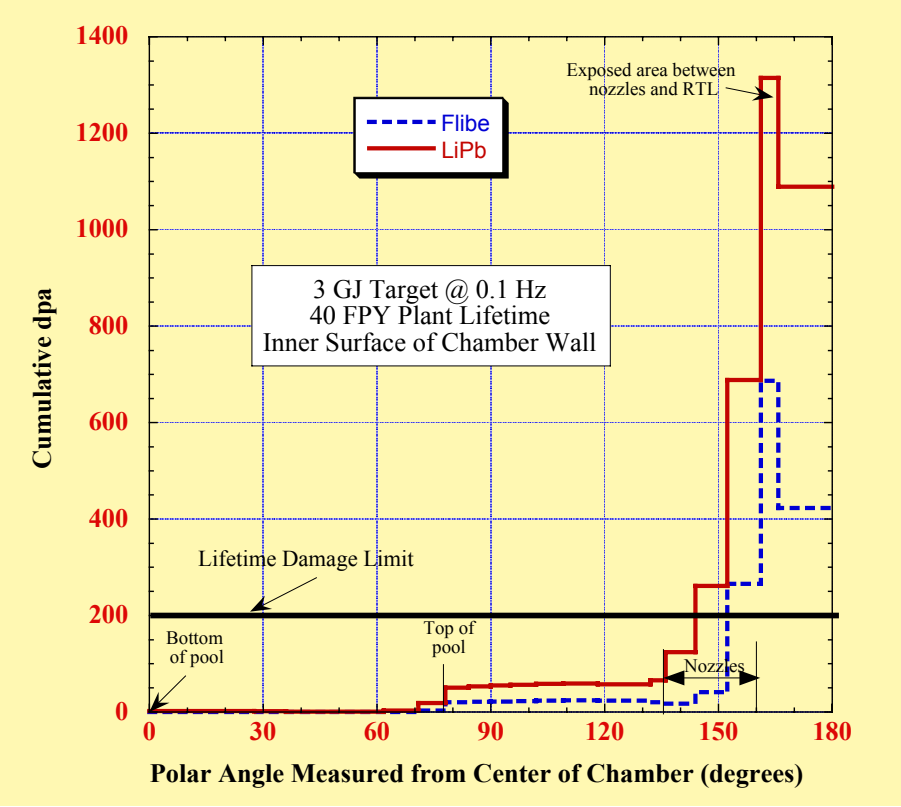

Fig. 19. Variation of cumulative radiation damage at inner surface of chamber wall.

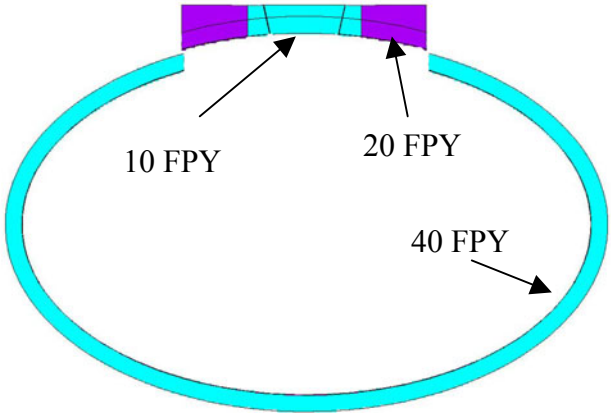

Chamber with Flibe

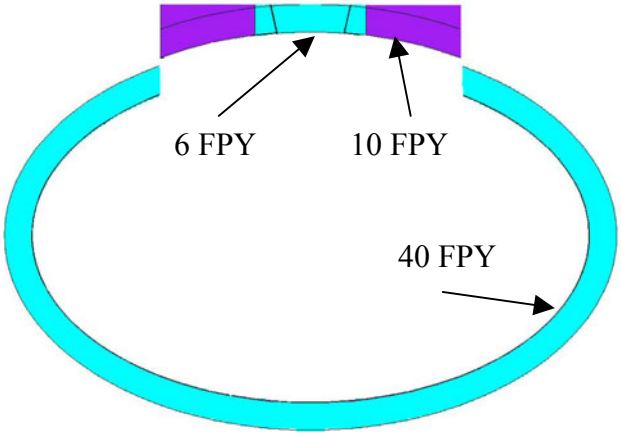

Chamber with LiPb

Fig. 20. Lifetime of chamber zones.

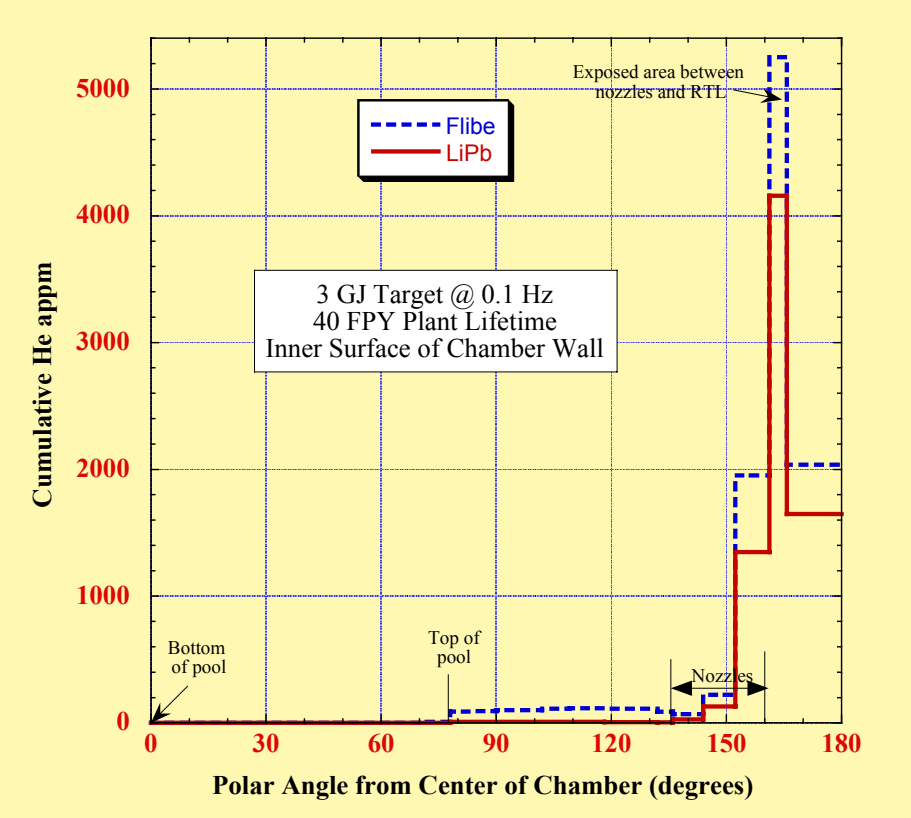

Fig. 21. Variation of cumulative helium production at inner surface of chamber wall.

3.2.5 Insulator shielding

As shown in Fig. 13, an insulator stack is located at the interface between the pulsed power driver and the coax conical RTL system. We calculated the absorbed dose and fast neutron (E > 0.1 MeV) fluence in the insulator stack located above the chamber with both Flibe and LiPb breeders. Performance of the insulators is very sensitive to radiation damage. The mechanical properties of organic insulators (epoxies and polyimides) degrade at absorbed doses larger than 10^9-10^{10} Rads [10]. Ceramic insulators are 2-3 orders of magnitude more radiation resistant than organic insulators. Candidate materials include Al_2O_3, MgO, and spinel ($MgAl_2O_4$). Spinel offers the lowest mechanical and structural degradation in a nuclear environment among its class of solid ceramic insulators. The fluence limit for ceramics is determined only by the maximum swelling to be tolerated. A maximum swelling of 3% is considered. This corresponds to fast neutron (E > 0.1 MeV) fluences of 1.1×10^{22} and 4×10^{22} n/cm^2 for MgO and spinel, respectively [11]. Table 6 lists the end-of-life organic insulator absorbed dose and fast neutron fluence for the chamber designs with Flibe and LiPb. Using LiPb results in about a factor of 5 higher insulator radiation levels. The absorbed dose in organic insulators is excessive and should not be used at these locations. On the other hand, if ceramic insulators are used, they are expected to survive for the entire plant lifetime.

Table 6. Absorbed dose and fast neutron fluence in the insulator after 40 FPY

	Flibe	LiPb
End-of-life (40 FPY) organic insulator dose (Rads)	4.4×10^{12}	2.0×10^{13}
End-of-life fast neutron fluence (n/cm^2)	1.4×10^{21}	6.4×10^{21}

3.2.6 Summary and conclusions

The 3-D neutronics calculations for the ZP-3 chamber indicate that the thermal power is ~6.5% higher when LiPb is used instead of Flibe. However, a 55% thicker jet zone is required with LiPb to provide adequate chamber wall shielding. A low lithium enrichment (20% ^{6}Li) in LiPb is adequate for tritium self-sufficiency. Both breeder options have the potential for achieving tritium self-sufficiency. Lithium enrichment can be used as a means for adjusting the TBR of LiPb, if needed. In both cases, the chamber wall does not need replacement except for the top part, including the nozzles, where the radiation damage is a factor of ~2 higher for LiPb. He production in the chamber wall protected by LiPb is much lower than that with Flibe. Rewelding is possible only in the lower part of chamber wall below the pool. About a factor of 5 higher insulator radiation level results with LiPb. Organic insulators cannot be used but ceramic insulators will survive for the entire plant lifetime of 40 FPY.

4. Idea for establishing jet flow in the ZP-3 chamber and preliminary thermal parameters

The present design work follows up on previous work developed in the past several years, but is guided by recently developed 3-D neutronics, which provides more accurate power distribution. Further, a detailed design of jet flow initiation and control has been developed. This entails the design of a mechanism, which initiates the flow of jets in the chamber just prior to the onset of a shot. The sequence of events in the chamber is described and parameters are given for the chamber, thermal hydraulics and power cycle.

4.1 Strategy for determining chamber protection and other parameters

One of the primary goals of the design is the protection of the chamber wall from damage by the neutrons with the aim of making it a lifetime component. This is done by 3-D neutronics, which determines the amount of fluid that is needed between the target and the chamber wall. At the same time, this amount of fluid should be adequate for breeding tritium, which is needed to fuel the reactor. Once this is determined, the arrangement of the jets can be made with respect to radial and circumferential spacing. It is important to realize that the amount of liquid in the jets should be adequate to protect the wall at the level of the target, which typically is two or more meters from the top of the chamber. Since the jets undergo thinning because their velocity is increasing, the liquid fraction at the target should be equal to that determined by nuclear analysis, and that fraction will be higher at the nozzles where the jets are initiated and lower on the bottom where the jets reach the pool. Once this information is determined, the nozzle pattern can be formulated. The hole pattern in the nozzle plate consists of holes arranged in successive circles at predetermined distances between holes in

any circumference and the distance between successive circles. The initial circumference defines the inner radius of the jets and the final one defines the outer radius. The initial velocity of the jets depends on the head provided above the nozzle plate and once that is determined, the drop time can be calculated, and from the velocity profile, the mass flow rate per shot can be determined. The design of the supply end can now proceed as well as the temperature rise in the jets and the pool. Finally, the mass flow rate to the heat exchanger can be set, as well as the pumping power both to the heat exchanger and within the chamber itself. From the predetermined power cycle efficiency, the total gross electric power is calculated and the net power determined by subtracting the necessary electric expenditures.

4.2 Design of the supply end and initiation of jet flow

Figure 22 is a cutaway of the chamber showing details of the upper section. The chamber is elliptical, 10 m in diameter and 6 m high. It consists of a conical structure (RTL) in the center, which holds the target at the apex of the cone, surrounded by the nozzle plate spanning a radial distance determined by the mass flow rate as prescribed by nuclear analysis. This is followed by a mechanism which allows the nozzle area to be flooded with fluid in a short time. This mechanism is called a sluice valve. Finally, the sluice valve is surrounded by an annular reservoir, which holds the fluid inventory needed to supply the jets for a single chamber shot.

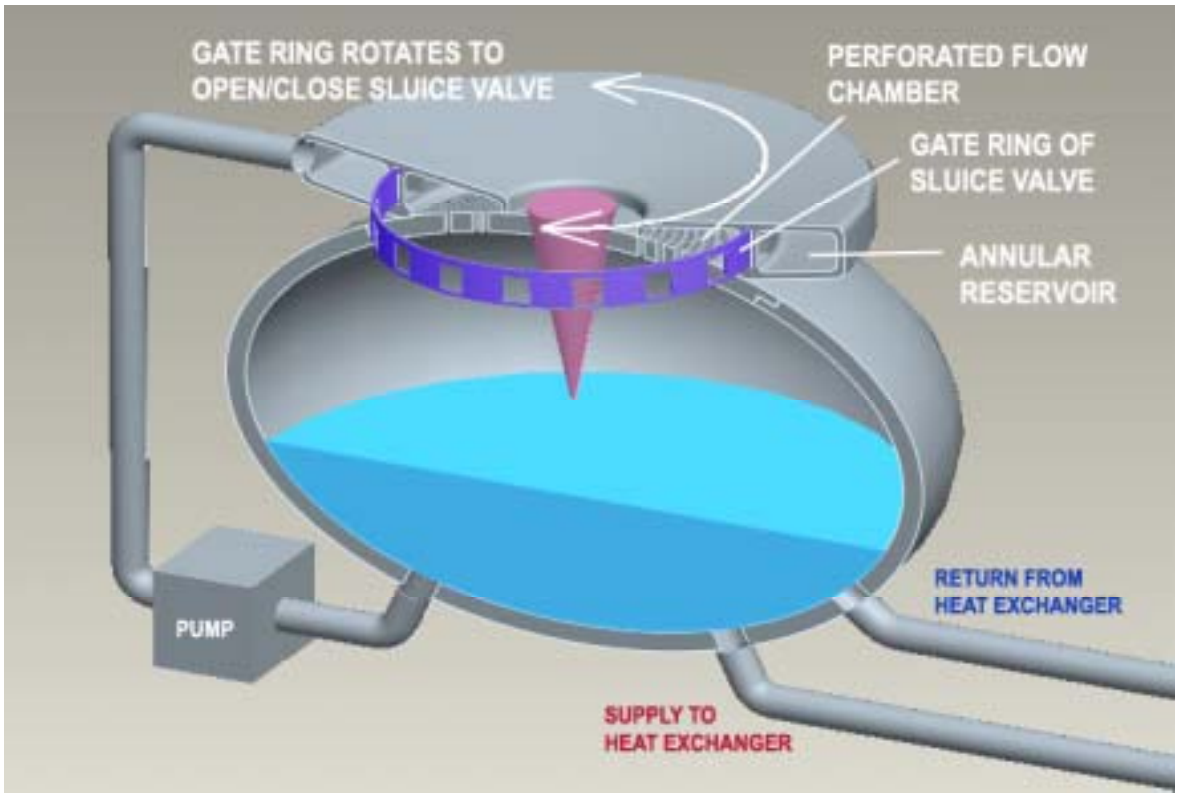

Fig. 22. Cutaway of the chamber showing details of the upper section.

4.3 Mechanical design of the sluice valve

The sluice valve, which separates the nozzle enclosure and the annular reservoir filled with fluid, consists of a series of rectangular openings connected with adjacent closures as shown in Fig. 22. In the closed attitude the closures seal off the openings in the annular reservoir. The jet flow is initiated by rotating the sluice valve several degrees of rotation. The amount of rotation depends on the sizes of the rectangular apertures and the corresponding openings in the annular reservoir. Typically, the flow area generated by the sluice valve should be equal to or greater than the flow area in the nozzles. The rush of the fluid into the nozzle enclosure starts the jets flowing. The design of this area is very critical, in order to insure that all the nozzles are supplied with fluid.

4.4 Start of jet flow, Z shot and immediately after

By estimating the initial jet velocity from the head above the nozzles, the time it takes for the jets to reach the pool is calculated. In this case, with the starting fluid velocity of 4.4 m/s at the nozzles, this time is 0.50 s. We estimate that it will take 3 s from the time the sluice valve is activated to the start of the jets; this implies that the shot should be set off ~ 3.5-4 s later. The pump, which supplies the annular reservoir from the chamber pool, runs continuously, even after the valve is open. This insures that fluid keeps flowing into the reservoir until the valve is closed and the reservoir is filled in preparation for the next shot. This implies that the pump (or pumps) should be sized to fill the reservoir in about 6 s. Another note worth mentioning here is that a sluice valve of this type is never seal tight but will allow some leakage. It is important to make sure that this leakage will not drip into the chamber during the time when the RTL is replaced. Therefore, the shape of the annular reservoir should allow some accumulation of fluid in it before the fluid reaches the nozzles. Table 7 gives an approximate time sequence during one pulse in the chamber.

Table 7. Approximate time sequence of events during one pulse.

TIME (s)	EVENT
1 – 6	Pump fills annular reservoir from chamber pool
2 – 2.5	Valve opens, fluid rushes to the jet nozzles
0.5	Jets reach the bottom pool
1	Z-pinch shot and shot mitigation

Figures 23, 24 and 25 show pictorially the sequence described above.

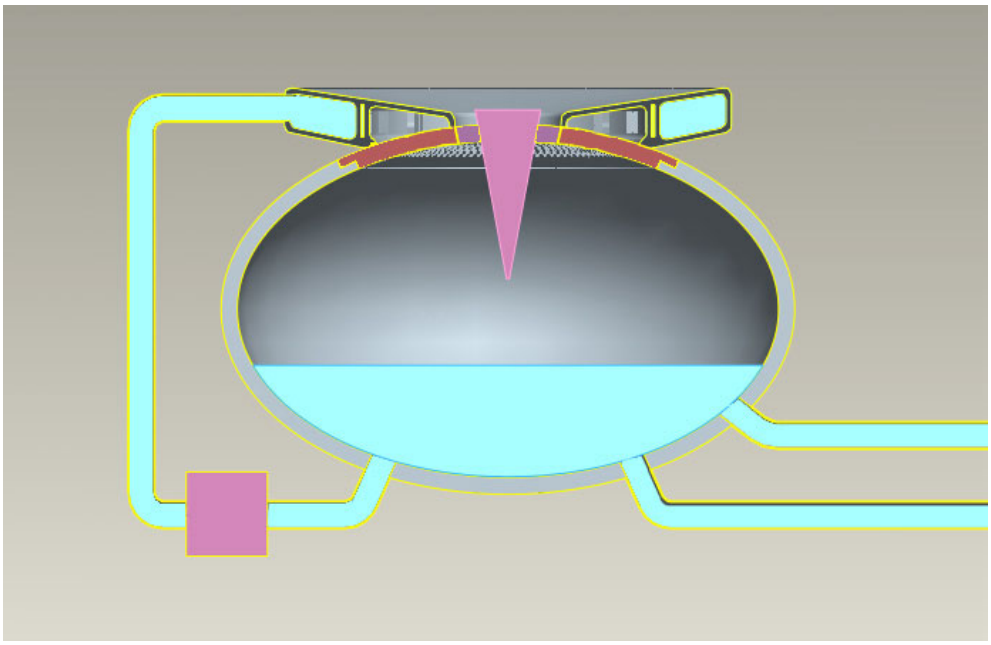

Fig. 23. Chamber just prior to opening of the sluice valve.

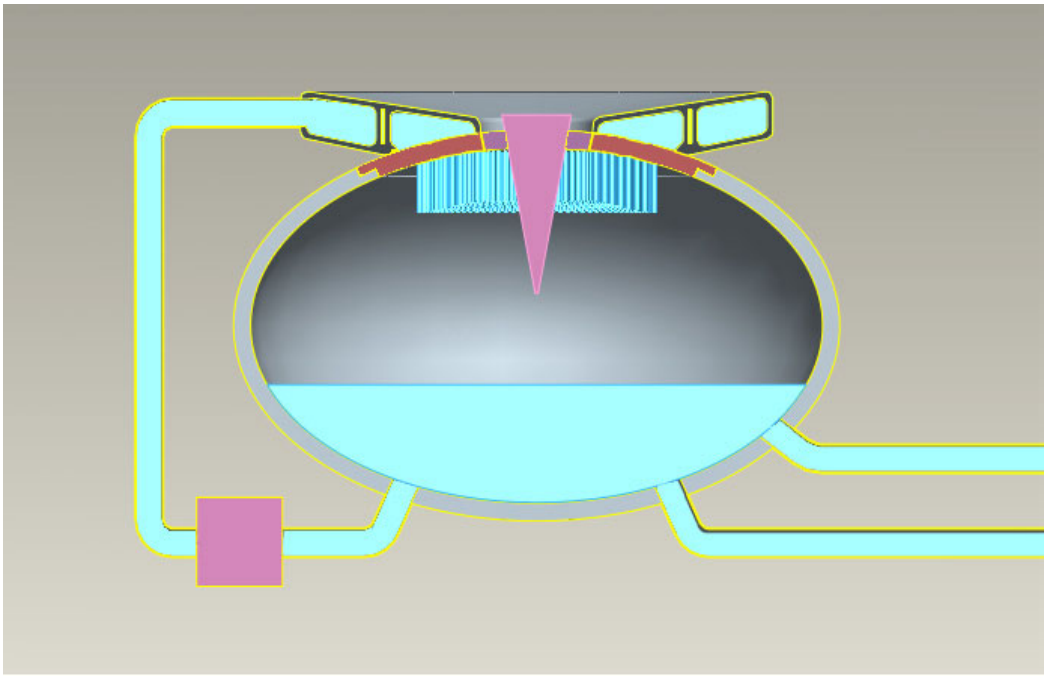

Fig. 24. Jet flow is initiated.

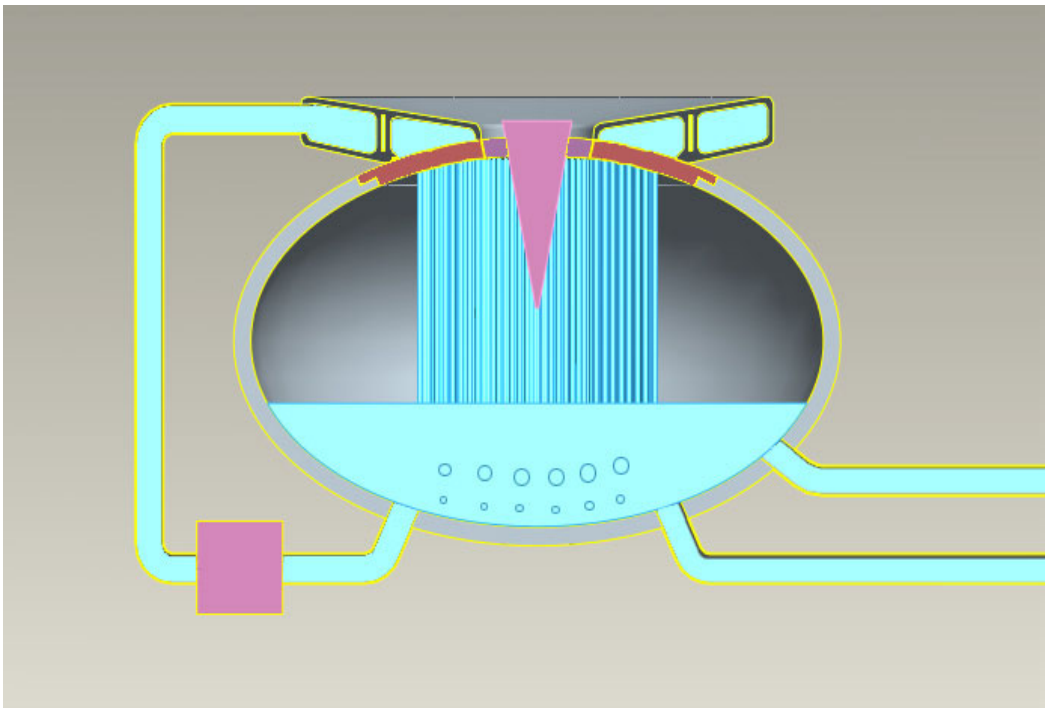

Fig. 25. Jets reach the bottom pool, which has He gas injected into it appearing as rising bubbles.

Figure 25 shows the jets reaching the bottom of the pool at which point the Z-pinch shot is set off and the jets are disassembled. The sluice valve is closed, but since there is still some fluid in the upper reservoir, the jets will persist until all the fluid drains out, typically in less than one second. The figure also shows gas bubbles rising in the pool. The intent of the bubbles is to make the liquid compressible, which aids in preventing a major shock from being transmitted to the chamber bottom.

4.5 Physical parameters of the ZP-3 chamber

As mentioned earlier, the chamber is elliptical, 10 m in diameter and 6 m high. The RTL extends 2 m below the nozzle plate, which means that the target is set off at that level. There are 562 nozzles in the Flibe case extending from a radius of 1.04 m to 2.06 m. In the case of LiPb, there are 1001 nozzles extending from 1.04 m to 2.64m. The radial and circumferential spacing is given in Table 8. The fluid fraction at the nozzles is 70%, but reduces to 37% at the target, 2 m below the nozzles.

Table 8. Preliminary physical parameters of the ZP-3 chamber for Flibe and LiPb

	Flibe	LiPb
Chamber diameter (m)	10.0	10.0
Chamber height (m)	6.0	6.0
Radius of first row of jets (m)	1.04	1.04
Radius of last row of jets (m)	2.06	2.64
Number of jet rows	8	12
Total number of jets	562	1001
Diameter of jets at the nozzles (cm)	12.5	12.5
Radial spacing between jet rows (cm)	14.5	14.5
Circumferential spacing between jets (cm)	13.9	13.9
Total fluid fraction at nozzles (%)	70	70
Fluid velocity at nozzles (m/s)	4.4	4.4
Diameter of jets at target (cm)	9.6	9.6
Total fluid fraction at target (%)	37	37
Fluid velocity at target (m/s)	7.7	7.7
Average drop distance of jets (m)	3.68	3.68
Time to traverse 3.68 m (s)	0.50	0.50
Diameter of jets at pool (cm)	8.5	8.5
Volume of fluid in jets per shot (m^3)	16.13	28.72

Table 8 gives the parameters of the chamber needed to compute fluid fractions at different levels in the chamber. The critical point is at the target, at a level of 2 m
below the nozzles. Three-dimensional neutronics has shown that the fluid fraction at this point needed to protect the chamber is 37%. The diameters of the jets in their fall from the nozzles keep getting smaller because of the increase of velocity. This is taken into consideration in calculating the volume of fluid exposed to the energy from the Z-shot.
Table 9 gives the preliminary thermal parameters of the chamber based on the fluid volume in the jets shown in Table 8.

4.6 Preliminary thermal parameters of the ZP-3 chamber

Table 9 gives the preliminary thermal parameters of the chamber, needed to calculate fluid temperatures as a result of the Z-pinch. The starting temperatures shown in Table 9 are dependent on the melting temperature of the fluid and the upper temperature value depends on the corrosion limit with respect to the ferritic steel structure. The low viscosity formulation of Flibe [$(LiF)_2.(BeF_2)$] has a melting temperature of 460^{o}C and its corrosion limit is ~ 700^{o}C. LiPb, on the other hand, has a melting temperature of 234^{o}C and a corrosion limit of 460^{o}C. For these reasons, the starting temperature for Flibe is 530^{o}C and the temperature at which the Flibe is taken to the heat exchanger is 680^{o}C. For LiPb, these temperatures are 275^{o}C and 450^{o}C respectively.

Table 9. Preliminary thermal parameters of the ZP-3 chamber

	Flibe	LiPb
Depth of fluid in the pool (m)	2.0	2.0
Fraction of gas in the form of bubbles in the pool (%)	20	20
Volume of fluid in the pool (m3)	66.6	66.6
Starting temperature in the pool (C)	530	275
Energy dissipated in jets (GJ)	2.685	2.692
Energy dissipated in the pool (GJ)	0.661	0.868
Temperature rise in jets per shot (C)	30.4	49.3
Temperature rise in the pool per shot (C)	2.1	6.9
Equilibrated temperature rise per shot (C)	8.3	19.7
Number of shots to reach operating temperature	18	9

The energy released in the Z-pinch is 3 GJ, but because of energy multiplication in the fluid, the total energy is somewhat higher. This can be seen in the sum of the energies dissipated in the jets and the pool, which are 3.346 GJ in the Flibe and 3.56 GJ in the LiPb.

Once the fluid in the jets mixes with the fluid in the pool, the equilibrated temperature is calculated to be 8.3^{o}C in Flibe and 19.7^{o}C in LiPb. These values determine the number of shots it takes for the fluid to reach operating temperature. Operating temperature is defined as that at which the fluid is transported to the heat exchanger for power conversion.

4.7 Power cycle parameters and possible thermal conversion cycle efficiencies

Table 10 gives the parameters of the power cycle. The Brayton cycle is used for Flibe because the temperature is high enough to justify its use. In this cycle, the Flibe exchanges heat with He gas, which is then used to drive a turbine. Figure 26 shows possible thermal cycles for a range of materials from 327^{o}C to 1227^{o}C. For Flibe, using the Brayton cycle at 953 K and 2 reheat stages, the estimated efficiency is 43.5%. On the other hand, for LiPb, a steam (Rankine) cycle is used at 700 K, also with two reheat stages, an efficiency of 41.9% is estimated. These efficiencies result in electrical power outputs of 145.6 MW_e for Flibe, and 149.2 MW_e for LiPb. Pumping power is calculated both within the chamber and that needed to transport the fluid to the heat exchanger. Within the chamber the fluid has to be lifted ~ 12 m, which accounts for the pipe bends. Both work in lifting the fluid and also friction are accounted for. It is assumed that the distance to the heat exchanger is 20 m. It can be seen the high density of LiPb accounts for a substantial increase in pumping power, which is especially evident when the fluid has to lifted, as in the chamber.

Table 10. Power cycle parameters of the ZP-3 chamber

	Flibe	LiPb
Power cycle	Brayton	Rankine
Fluid temperature to heat exchanger (C)	680	450
Fluid return temperature from heat exchanger (C)	530	275
Thermal power supplied by chamber during a pulse (MWth)	334.6	356.0
Mass flow rate to heat exchanger (kg/s)	940	10,170
Pumping power within a chamber (MWe)	1.0	8.16
Pumping power to heat exchanger (MWe)	0.9	3.7
Power cycle efficiency (%)	43.5	41.9
Electric power generated per chamber (MWe)	145.6	149.2
Electric power less pumping power (MWe)	143.1	137.3

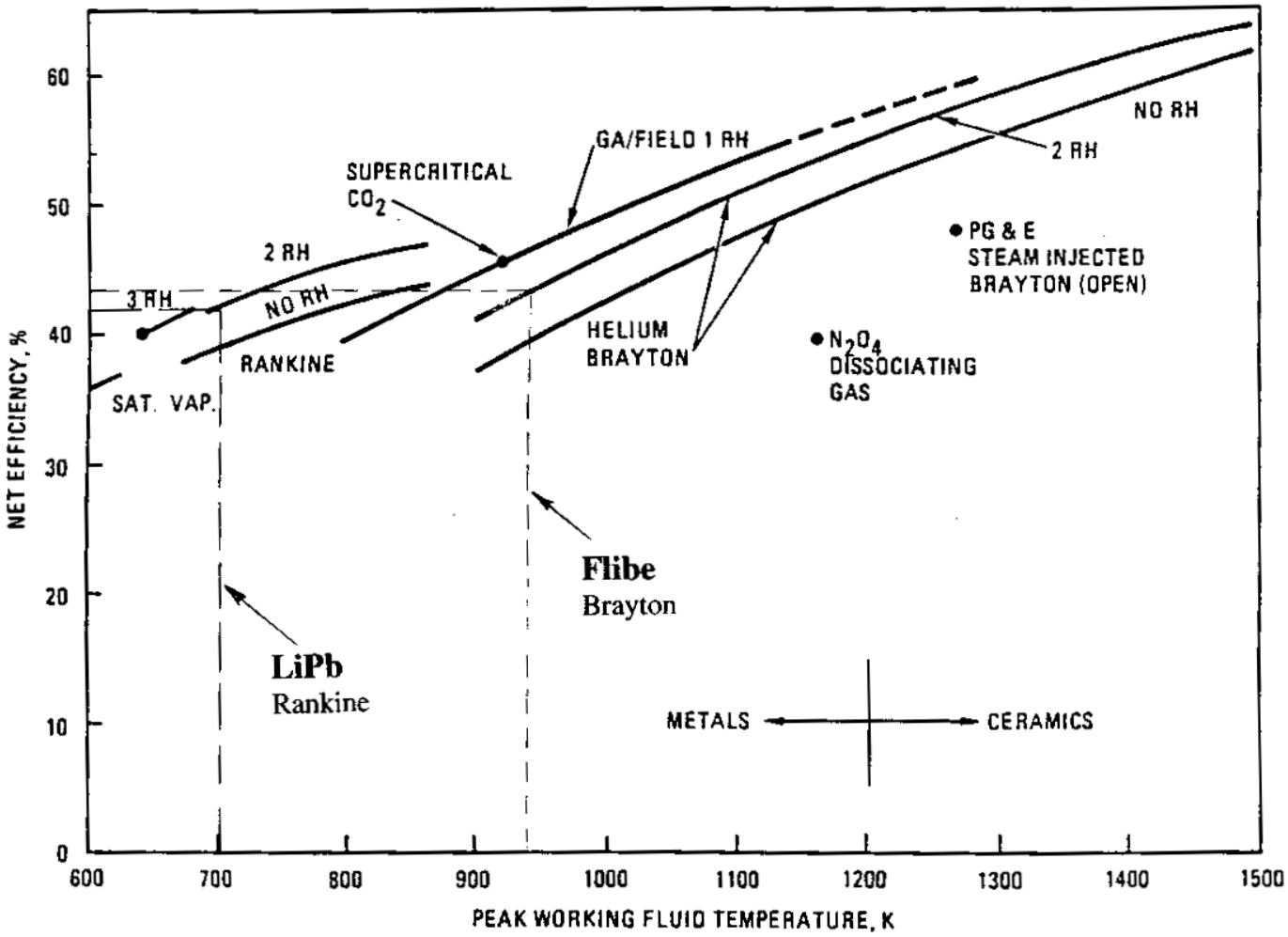

Fig. 26. Possible thermal cycle conversion efficiencies (courtesy of R. Bourque - GA).

5. Activation and radwaste classification

Another topic that has been investigated jointly by the 1-D and 3-D analyses is the activation of the chamber wall. This was assessed in two steps. First, the 1-D simple spherical model along with the ALARA pulsed activation code [12] was used to check the radwaste level of the candidate steels: A-286 and F82H. The DANTSYS code [6] produced the input flux file for the individual pulses for ALARA using a neutron yield of 1.1×10^{21} n/pulse. The 2.68 million pulses per year combined with the 85% projected system availability formed the basis for the irradiation history for ALARA. Second, the overall WDR of the chamber wall was estimated using the 3-D analysis where the spectral neutron flux for each chamber wall segment was coupled with the ALARA activation code. Use is made of the recommended service lifetimes (refer to Fig. 20) to specify the irradiation time for each segment.

Figures 27 and 28 demonstrate the WDR of the chamber wall segments located behind the Flibe and LiPb jets, respectively. This life-of-plant segment will generate high-level waste (WDR >> 1) if made of A-286 steel, even if placed at a fairly large distance (> 5 m) away from the jets. The dominant radionuclide is ^{99}Tc ($T_{1/2}$= 2.1×10^5 y) from the Mo alloying element. Reducing the Mo content to enhance the WDR may jeopardize the mechanical properties of the A-286 steel. On the other hand, the F82H steel looks promising as its WDR exceeds the Class-C LLW limit by a factor of a few. The dominant radionuclides are ^{94}Nb ($T_{1/2}$= 2×10^4 y) and ^{99}Tc from Nb and Mo impurities, respectively. Controlling these impurities would easily qualify the F82H steel as Class C LLW waste.

The neutron flux and activation responses vary greatly as one moves along the perimeter of the chamber wall. Thus, we estimated the overall WDR by coupling the 3-D flux with ALARA, taking into account the volume and service lifetime of each segment. The overall WDRs averaged over all segments are summarized in Table 11. Clearly, the A-286 steel cannot meet the low-level waste requirement (WDR < 1). This activation problem has ruled out the A-286 steel from further consideration. A chamber wall made of F82H steel can qualify as Class-C LLW (WDR < 1) with Nb and Mo impurity control. If feasible at a reasonable cost, the LLW design requirement will be met with a wide margin.

Table 11. Overall waste disposal rating for the chamber wall

	Flibe	**LiPb**
A-286 Steel	117	195
F82H Steel	1.0	1.7

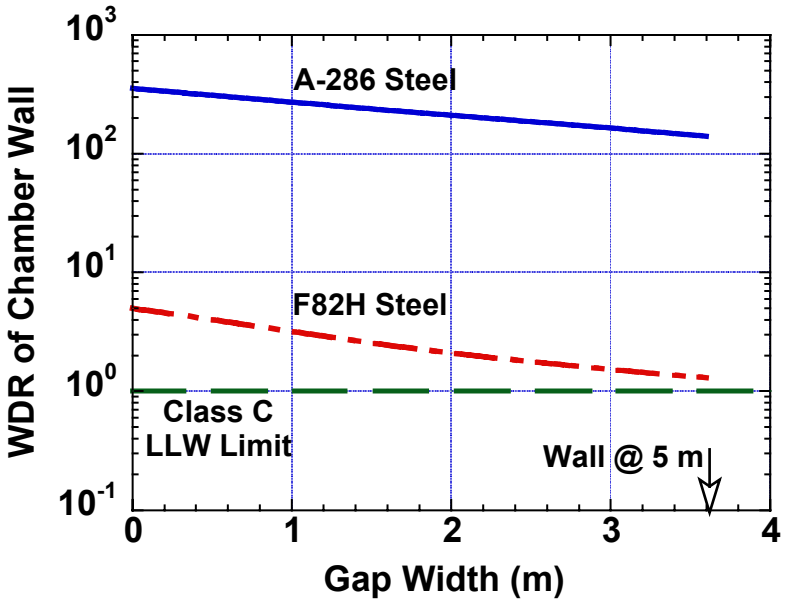

Fig. 27. Reduction of WDR with gap between Flibe jets and chamber wall.

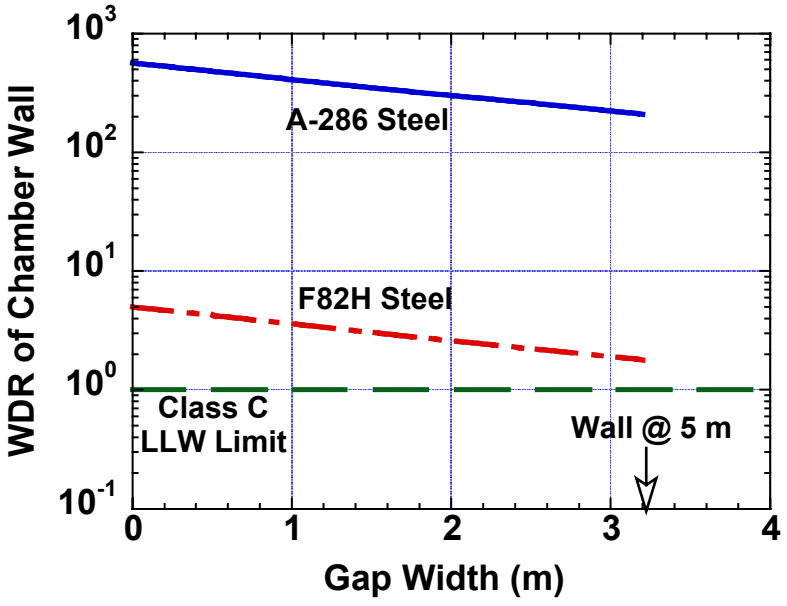

Fig. 28. Reduction of WDR with gap between LiPb jets and chamber wall.

6. Flibe / LiPb system comparison

The selection criteria for the preferred breeder should include several elements that play an essential role in the acceptability of the breeder. These are the compatibility with the FS structure, nuclear performance, stability under irradiation, operating temperature window, power conversion efficiency and net power output, safety characteristics, and impact on the overall cost of electricity (COE). It would be relatively simple to achieve attractiveness for a few elements, but it will be a challenge to achieve attractiveness for all elements. Each of the candidate breeders ($Li_{17}Pb_{83}$ liquid metal and F_4Li_2Be molten salt) has its own benefits and design challenges. Historically, the Flibe breeder has been employed by the IFE OSIRIS and HYLIFE-II type studies as well as the MFE Japanese stellarator project, while numerous IFE and MFE designs utilized the LiPb breeder.

There are two ways to proceed with the Z-pinch study: 1) select a breeder early and develop a complete design with detailed assessment, drawings, cost, etc., and 2) delay the breeder selection process, consider the two breeders for a year (or more), address the critical issues, and develop innovative solutions for outstanding problems. The first option looks less appealing while the second will benefit the Z-pinch program and deliver a credible design.

From its very inception, the Z-pinch project selected steel as the main structure for the chamber wall. Advanced steels can withstand a relatively high temperature (> 550°C), a property of high payoff. The steel temperature limits are set by the mechanical properties, breeder's corrosion and compatibility issues, irradiation effects, etc. The higher the steel temperature, the higher the breeder output temperature, and thus the higher the power conversion efficiency (refer to Fig. 26). The desire for high-temperature steels inspired the materials community and steel industries to develop advanced steels suitable for service at 800–1000^{o}C [5,13,14]. At present, establishing more definitive temperature limits is difficult as such advanced steels are currently under development for nuclear applications. It seems likely that the advanced steel database will be established over the next 10-20 years and, hopefully, become available before the Z-machine is built.

The following tables summarize the key features, benefits, and issues for each breeder. Table 12 compares the breeders on the basis of the engineering and economic parameters. A 55% thicker LiPb jet zone is required to protect the chamber wall (refer to Section 3.2). Despite the thicker jets, the LiPb volume differs by only 10% as the pool dominates the in-chamber volume. The effect of the more expensive Flibe counterbalanced the effect of the more massive LiPb and the total breeder cost is \$140M for Flibe and \$170M for LiPb, only a 20% difference.

Table 12. Impact of breeders on selected engineering and economic parameters

	Flibe	**LiPb**
Thickness of jet zone	1.1 m	1.7 m
Overall TBR	1.1	1.1
Li enrichment	Natural	20%
Overall energy multiplication	1.1	1.2
In-chamber volume* (m^3)	800	900
Total volume# (m^3)	1600	1800
Unit cost ($/kg)	43	10
Total cost (M$)	140	170

* 100% dense breeder; 10 units.

\# Inside and outside the chambers. Assuming outer loop contains same breeder volume as in all 10 chambers.

Table 13. Impact of breeders on selected chamber wall parameters and radwaste stream

	Flibe	**LiPb**
Wall thickness (cm)	30	50
Peak dpa @ EOL	200	200
Lifetime (FPY)	10, 20, 40	6, 10, 40
Top reweldable?	No	No
Waste classification	HLW - A286 steel LLW - F82H steel	
Waste volume (m^3) - 10 units:		
Replaceable components (6-20 FPY)	150	480
Permanent components (40 FPY)	630	1060
Total over plant life	780	1540
Building volume (m^3)	~2 x 10^5	~2 x 10^5

The impact of the breeders on the chamber wall parameters and radwaste stream is given in Table 13. A thicker chamber wall is required with LiPb to reduce nuclear heat leakage to < 1% (refer to Section 3.1). The LiPb option generates almost twice the life-cycle FS radwaste. However, the 10 chamber walls represent only ~1% of the building waste.

Table 14 compares the two breeders and the conventional and advanced steels on the basis of the anticipated impact on the operating temperature and net electric power output. The assumptions made are included in the footnotes. Both Flibe and LiPb breeders have a compatibility problem that controls the interface temperature with steels. Means to raise the interface temperature include: 1) coating the steel with a thin, plasma sprayed layer of W, and 2) plating the steel with a thin layer of Ta using plasma spraying or explosive welding techniques [15]. Fabrication of the nozzles from W would alleviate the corrosion/erosion problem.

The coated ODS steel offers higher operating and breeder outlet temperatures compared to the conventional F82H steel. Advanced power cycles with efficiencies approaching 50% look very attractive. Excluding the 2 and 12 MW_e pumping powers (see Table 10) for Flibe and LiPb, respectively, ~170 MW_e driver power, ~200 MW_e for RTL fabrication plant, and ~50 MW_e miscellaneous power, the net electric power for the Flibe and LiPb systems are comparable for the advanced ODS steel case. The LiPb system generates ~150 MW_e more power for the conventional F82H steel case. Note that the higher thermal power of the LiPb system more than offsets its factor of six higher pumping power. Regarding the external piping, suitable high-strength and high-temperature alloys will be needed. The ORNL fusion materials program is currently performing scoping studies on LiPb with superalloy, a candidate piping material outside the power core [16]. No compatibility tests with Flibe are taking place at ORNL. However, some general information on Flibe compatibility is available from work performed at INL [17].

Table 14. Impact of breeder and steel type on operating temperature and power output

	Flibe		**LiPb**	
Steel type	F82H	ODS[#*]	F82H	ODS[#*&]
Steel T_{max}	700°C	800°C	550°C	800°C
Breeder/steel interface T_{max}	~700°C	< 800°C	500-550°C	< 800°C
Breeder T_{out}	≤ 680°C[+]	750-800°C[+]	< 550°C[@]	750-800°C[+]
η_{th}	40-45%	~50%	40-45%	~50%
P_{th} (MW_{th}/chamber)	335	335	356	356
P_G (MW_e/chamber)	134-151	~168	142-160	~178
P_e (MW_e/chamber)	132-149	~166	130-148	~166
Gross power (10 units)	1320-1490	~1660	1300-1480	~1660
Net electric power (10 units)	900-1070	~1240	880-1060	~1240
Need cleanup system?	Yes[**]		Yes[##]	

Advanced oxide dispersion strengthening (ODS) steel with nano-sized TiO_2 and Y_2O_3 particles, offering high operating temperature and strength. Assuming 200 dpa limit @ 800°C.
* If plated with 1 mm W (or Ta) or coated with 10 microns alumina; W nozzles.
@ Rankine power conversion cycle (for T < 600°C).
\+ Brayton power conversion cycle (for T > 650°C).
% Assuming 170 MW_e driver power, 200 MW_e for RTL fabrication plant, 50 MW_e miscellaneous power.
& Oxygen should be excluded.
** For REDOX chemistry control and separation of RTL/target debris.
To limit Bi and Po concentrations and separate RTL/target debris.

Flibe dissociates under irradiation and has a compatibility problem with FS if the radiolysis byproducts cannot be controlled by chemical means. Neutrons interact with Flibe and produce the extremely corrosive free fluorine and the less corrosive tritated hydrofluoric acid (TF) [18]. A reduction and oxidation (REDOX) agent, such as beryllium, is essential for the viability of the Flibe breeder to control the free fluorine and TF and minimize the corrosion

[19]. As successfully demonstrated for the fission molten salt program, the use of Be as a REDOX agent and the kinetics of the basic reactions need to be demonstrated for fusion applications. Experimental work on REDOX to limit the corrosive effects of F and TF is being performed at INL as part of the US-Japan Jupiter-II program [17].

A radiological concern for the LiPb breeder arises from the neutron-induced ^{210}Po and ^{203}Hg radionuclides. The ^{209}Bi inventory is also of interest because, as a precursor to ^{210}Po, control of its concentration to 10 appm can serve as a mechanism to limit the ^{210}Po inventory. An online purification system is necessary to remove the ^{210}Po and/or ^{209}Bi generated by Pb during operation [20].

Additional advantages and drawbacks for both breeders are listed in Table 15. Both systems have low tritium inventory, but the control of the tritium permeation to the environment (external pipes, heat exchanger, etc.) will be more of a concern for Flibe. Another point of concern relates to the Flibe steep radial profile and large temperature gradient. These features lead to a violent event following the target implosion. Rodriguez's analysis indicates Flibe components reach as much as 10000 m/s for a fraction of a second, then slow down to 750 m/s, hitting the remaining part of RTL [21]. LiPb may offer an advantage in this regard as the pool may hardly move. This issue should be investigated.

7. Conclusions and future work

Several important engineering features have been incorporated to improve the Z-pinch performance. For instance, advanced high-temperature steel-based structure could operate near 800^{o}C, advanced power cycle could achieve high thermal conversion efficiency approaching 50%, low-activation F82H steel with controlled Nb and Mo impurities will generate only low-level waste, and an innovative idea has been developed to establish the jet flow using a sluice valve.

We performed detailed assessments for the two candidate breeders (Flibe and LiPb) in the nuclear, activation, thermal, and power conversion areas. A comparative study, highlighting the pros and cons of both breeders, covered the chamber dimensions, breeder properties and performance, and impact on the net output power. The study suggests that:

- Both Flibe and LiPb breeders are technically feasible for the Z-pinch concept, breeding sufficient tritium and protecting the chamber wall
- The volume (and cost) of the breeder and chamber should be valued low compared to other criteria
- The chemistry control by REDOX tops the list of critical issues for Flibe. Its dissociation under Z-pinch operating conditions needs further evaluation
- Bi and/or Po control system is required for the LiPb option

On common design issues for both breeders, the following items need to be addressed in the future:

- Inventories: F, TF, ^{16}N for Flibe and ^{210}Po, ^{209}Bi, and ^{203}Hg for LiPb
- Tritium extraction, permeation, and migration

- Feasibility of lining the chamber wall with 1 mm W using plasma spraying or explosive welding techniques

Table 15. Advantages and disadvantages of Flibe and LiPb breeders

	Advantages	Disadvantages
Flibe:		
	- Good shielding performance	- More expensive than LiPb
	- Light weight	- High melting temperature (460^{o}C); small temperature window with F82H steel
	- Low pumping power (2 MW_e)	
	- Low-pressure operating system	- High viscosity
	- Very low tritium solubility; low tritium inventory	- Tritium permeation and control is a serious issue
	- Relatively inert with air and water	- Low thermal conductivity
		- Limited heat transfer capability
		- Very corrosive in radiation environment
		- REDOX chemistry control is needed
		- Very steep radial power profile and large temperature gradient
		- Pool shoots up at high speed (> 750 m/s), hitting remaining RTL
		- Limited database
LiPb:		
	- Lower T partial pressure than Flibe	- Lower shielding performance compared to Flibe
	- Low tritium solubility; low tritium inventory	- Heavy weight
	- Generate more thermal power than Flibe	- 12 MW_e pumping power
		- Tritium permeation and control is an issue
	- React mildly with water	- Need online Po and/or Bi removal system
	- Higher heat conductivity than Flibe	- Corrosive
	- Less steep radial power profile and temperature gradient than Flibe	
	- Suppress shock wave; pool may hardly move	
	- Lower melting temperature (234^{o}C); large temperature window	
	- Less expensive than Flibe	
	- Large database from ITER and Gen-IV	

Acknowledgments

The authors wish to thank R. Peterson, S. Rodriguez (Sandia National Laboratories), S. Zinkle (Oak Ridge National Laboratory), and S. Malang (Germany) for the helpful discussions and useful comments in preparing this document.

References

[1] C. Olson, G. Rochau, M. Matzen et al., "Z-Pinch IFE Program – Final Report for FY04," Sandia National Laboratories Report, SAND-2005-2742P (April 2005).

[2] Allegheny Ludlum Altemp A-286 Iron-Based Superalloy. Specs available at: http://www.alleghenyludlum.com

[3] R. Klueh et al., "Impurity Effects on Reduced-Activation Ferritic Steels Developed for Fusion Applications," Journal of Nuclear Materials 280 (2000) 353-359.

[4] S. Zinkle, J. Robertson, and R. Klueh, "Thermophysical and Mechanical Properties of Fe-(8-9)%Cr Reduced Activation Steels," Fusion Materials Semiannual Progress Report for the Period Ending June 30, 2000 (DOE/ER-0313/28), pp. 135-143 (2000).

[5] G.R. Odette and D.T. Hoelzer, "Development of Nanocomposited Ferritic Alloys for High Performance Fusion First Wall and Blanket Structures," ANS-FED newsletter, June 2002. Available at: http://fed.ans.org/

[6] DANTSYS: A Diffusion Accelerated Neutral Particle Transport Code System, Los Alamos National Laboratory, LA-12969-M (June 1995).

[7] M. Herman and H. Wienke, FENDL/MG-2.0 and FENDL/MC-2.0, the processed cross-section libraries for neutron-photon transport calculations, Report IAEA-NDS-176, International Atomic Energy Agency (March 1997).

[8] X-5 Monte Carlo Team, "MCNP-A General Monte Carlo N-Particle Transport Code, Version 5-Volume II: Users Guide," LA-CP-03-0245, Los Alamos National Laboratory (April 2003).

[9] D. Lopez Aldama and A. Trkov, "FENDL-2.1, Update of an Evaluated Nuclear Data Library for Fusion Applications," Report INDC(NDS)-467, International Atomic Energy Agency (December 2004).

[10] M. Sawan and P. Walstrom, "Superconducting Magnet Radiation Effects in Fusion Reactors," Fusion Technology 10/3, 741 (1986).

[11] G. Hurley et al., "Structural Properties of MgO and $MgAl_2O_4$ After Fission Neutron Irradiation Near Room Temperature," LA-UR 81-2078, Los Alamos National Laboratory (1981).

[12] P. Wilson and D. Henderson, "ALARA: Analytic and Laplacian Adaptive Radioactivity Analysis Code Technical Manual," University of Wisconsin Fusion Technology Institute, UWFDM-1070 (1998).

[13] M. Billone, R. Raffray, D.K. Sze, and L. El-Guebaly, "ARIES Assessment of IFE Structural Material," University of California San Diego Report UCSD-ENG-101 (2002).

[14] C. Kelber, "Inadequacy of Gen IV?," Nuclear News, Letters to the Editor, Page 10, July 2005.

[15] S. Malang, Consultant, Germany, private communications (July 2005).
[16] S. Zinkle, ORNL, private communications (July 2005).
[17] D.A. Petti, G.R. Smolik, M.F. Simpson et al., "An Update on the JUPITER-II Molten Salt Flibe Tritium, Chemistry and Safety Experimental Program," To be published in Fusion Engineering and Design.
[18] M. Sawan and D-K Sze, "Transmutation and Production Rates of Elements in Flibe and Flinabe with Impact on Chemistry Control," Fusion Science and Technology 44, 59 (2003).
[19] C. Wong, S. Malang, M. Sawan et al., "Assessment of First Wall and Blanket Options with the Use of Liquid Breeder," Fusion Science and Technology 47, 502 (2005).
[20] D. Henderson, L. El-Guebaly, P. Wilson, and A. Abdou, "Activation, Decay Heat, and Waste Disposal Analysis for ARIES-AT Power Plant," Fusion Technology, 39, No. 2, 444 (2001).
[21] S. Rodriguez, SNL, private communications (October 2005).